Transilvania
University
of Brasov

INTERDISCIPLINARY DOCTORAL SCHOOL

Faculty of Mechanical Engineering

Eng. Claudiu NEDELESCU

The research of applicable technical solutions for mitigating vehicle occupants' injuries in the event of an impact with a rigid barrier

SUMMARY

Scientific supervisor

Prof.Dr. Anghel CHIRU

BRASOV, 2025

Table of Contents

ABSTRACT

Road accidents are one of the leading causes of loss of human lives and serious injuries globally. They have significant consequences for public safety and the economy. In this context, ensuring the safety of vehicle occupants remains a major concern, and the development of technical solutions to reduce collision severity represents an important area of research. This thesis aims to investigate technical solutions applicable for mitigating injuries of vehicle occupants in the event of a frontal impact with a rigid barrier and includes the proposal of a damping system designed for their protection.

The necessity of this research is supported by statistics showing a high rate of severe accidents, as well as by increasingly strict international regulations regarding vehicle safety. In this context, the main objective of the thesis is to design a technical solution that contributes to reducing the forces transmitted to occupants during impact. To achieve this objective, the research included both theoretical and experimental analysis of the vehicle-barrier impact, using specific methods such as mathematical modeling, numerical simulation, and testing.

The first stage of the studies consisted of an analysis of the current state of research regarding the frontal impact between a vehicle and a rigid barrier, including general aspects related to road accidents, relevant national and international statistical data, as well as specific regulations concerning occupant safety. Also, current experimental research directions were examined, including the methods used to investigate this type of impact and well-established experimental approaches. Fundamental theoretical concepts related to impact mechanics, vehicle dynamics, biomechanical criteria used in injury assessment, and the role of passive safety systems were also analyzed. This synthesis provided a solid basis for developing the mathematical model, conducting numerical simulations, and interpreting experimental results.

Subsequently, the mathematical modeling of the frontal impact was carried out by developing a system based on masses, springs, and dampers. This proved useful in describing the behavior of the vehicle and its occupants during the collision. The equations of motion were determined and then modeled in Simulink. They were used to analyze the behavior of the system under impact conditions. Also, to support the finite element analysis, theoretical concepts from analytical mechanics were studied, comparing the Lagrange and Gibbs-Appell methods. It was observed that the use of the Gibbs-Appell method requires fewer differentiations, which leads to a reduction in the amount of calculations needed during the analysis process. For this purpose, a numerical model was developed using the finite element method to study the frontal collision between a vehicle equipped with a damping system and a rigid barrier. The construction and discretization of the model were performed in the Hypermesh software environment, part of the Altair Hyperworks suite, and the analysis was carried out using the RADIOSS solver. The interpretation of the resulting data was performed using the Hyperview and Hypergraph applications, allowing for a detailed assessment of the structural behavior of the vehicle under impact conditions.

In the thesis, the equipment, software applications, and procedures used for the acquisition and processing of experimental data are presented. Based on the previous analyses, the experimental research methodology was developed, including the preparation of the experiments, the establishment of impact conditions, and their execution. The tests were conducted for two distinct scenarios: a vehicle equipped with the proposed damping system and a standard vehicle, both involved in a frontal collision with a rigid barrier. In each test, instrumented dummies were used, and the data were evaluated using acceleration sensors and specialized software applications.

The analysis and processing of the experimental data provided the kinematic parameters of the vehicle and occupants for both testing scenarios. The comparative analysis showed a significant reduction in the forces transmitted to the occupants when using the damping system, particularly for the rear passenger, where the distribution of impact forces was optimized. Based on the kinematic parameters, biomechanical injury criteria such as HIC 36 and ThAC were calculated to evaluate the effects of the

impact. Finally, the mathematical model was calibrated and validated by comparing the results of the numerical simulations with the experimental data, revealing a relevant correlation for impact analysis.

The conclusions of the research highlight the applicability of the technical solution in the field of vehicle safety. They confirm that the use of a damping system mounted in the bumper of a vehicle can contribute to reducing the severity of frontal impacts on occupants. The proposed research methodology can constitute a basis for future studies on other types of collisions and innovative damping materials.

1 CURRENT STATE OF RESEARCH IN THE FIELD OF ROAD TRAFFIC ACCIDENTS

1.1 General Aspects Regarding Road Traffic Accidents

A road accident can be defined as an unpredictable circumstance involving at least one hazardous event, manifested by physical injuries to the occupants or damage to the vehicle involved. In general, an unforeseen event is characterized by the fact that it goes beyond the scope of human control. Such an incident arises at the moment control is lost and ends either with its restoration or, in the absence of intervention by individuals capable of regaining control, with the degradation of all goods [1].

1.2 Statistics on Road Traffic Accidents

1.2.1 Statistics on Road Traffic Accidents in Romania

Road accidents continue to cause a large number of deaths in Romania, the country with the highest number of victims resulting from such events in the European Union.

In 2024, ERSO (European Road Safety Observatory) published the report "Country Overview 2024: Romania", which highlights that in 2021, Romania recorded 1,779 deaths and 3,796 people seriously injured in road accidents. Regarding the road mortality rate, the document underlines that Romania had in 2021 the highest level in the European Union, with 93 deaths per million inhabitants.

The analysis of the evolution for the period 2012–2021 shows that the reduction in the number of fatalities in Romania was only 13%, far below the European Union average, which reported a 25% decrease during the same period, Figure 1.1.

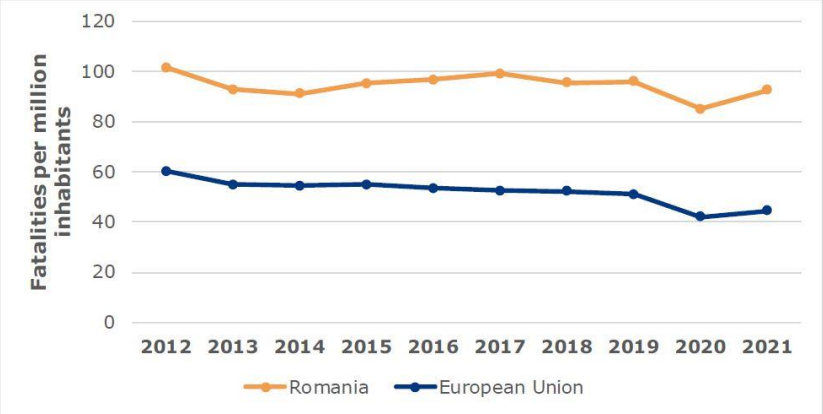

Figure 1.1 Evolution of the mortality rate, 2012–2021, comparison Romania vs. EU [2]

However, the number of seriously injured people recorded a more significant decrease of 57%, with the most significant drops in 2020 and 2021.

This aspect could largely be explained by the national restrictions imposed in the context of the COVID-19 pandemic, which limited travel to the strictly necessary, rather than by the effects of infrastructure improvements or awareness campaigns implemented as part of national public policies [2].

1.2.2 Global Statistics on Road Traffic Accidents

According to a report published by the World Health Organization (WHO) in 2023, the estimated number of deaths caused by road accidents worldwide in 2021 was 1.19 million, which corresponds to a rate of 15 deaths per 100,000 inhabitants. This value represents a reduction of approximately 5% compared to the estimates from 2010, when 1.25 million traffic deaths were recorded. This reduction can be partly attributed to the implementation of the “Decade of Action for Road Safety 2011–2020.”

The number of victims in road accidents peaked in 2012, with 1.26 million deaths, followed by a progressive decline starting in 2013 and continuing until 2021 (Figure 1.2). A notable deviation from this downward trend was observed in 2020, when global mobility restrictions imposed to manage the COVID-19 pandemic led to a significant but temporary reduction in road deaths [3].

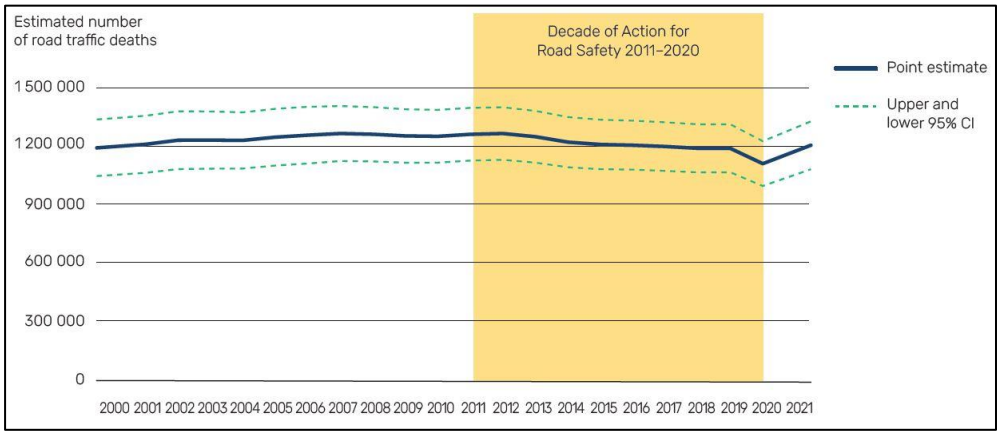

Figure 1.2 Number of road traffic deaths during the period 2000–2021 [3]

IIHS published a study in 2021 showing that a significant proportion of road traffic fatalities, estimated at 20%, is attributed to vehicles leaving the roadway and striking fixed objects along the road. Among the most frequently involved objects in such crashes are trees, poles, and guardrails. Nearly half of these fatal incidents occur at night, when reduced visibility contributes to increased risks [4].

1.3 International Regulations and Standards on Road Safety

1.3.1 Vehicle Safety Assessment

The European New Car Assessment Programme (Euro NCAP) aims to provide an accurate and objective evaluation of the safety level of vehicles, thus supporting consumers in making purchasing decisions. The program focuses on testing the most popular car models marketed in the European Union and functions as a partnership between the public and private sectors, being independent of type-approval procedures [5].

An additional method of assessing vehicle safety consists of periodic technical inspection, whose main objective is to reduce the number of vehicles that may have current or potential defects contributing to road accidents [6].

1.3.2 Vehicle Safety Standards

An essential principle of legislative technical regulations is to avoid imposing strict design requirements, favoring instead the establishment of clearly defined performance criteria, to be evaluated through type-approval tests.

At the global level, perspectives on vehicle safety regulations differ significantly. In the United States, the competent authorities have argued that the education of road users, especially drivers, has a limited impact on their behavior. For this reason, priority was given to passive protection systems, designed to reduce injuries in the event of an accident, while accident prevention measures were placed in the background.

In contrast, European regulations have promoted a different approach, placing greater responsibility on drivers. European legislation has focused mainly on proactive measures aimed at preventing accidents by promoting active safety and responsible behavior in traffic [7-9].

1.4 Current Experimental Research on Vehicle-Rigid Barrier Impact

Recent studies present various dummies used to study the degree of head injury. For example, in a study published in 2019 [10], a prototype dummy head was evaluated using a test platform that records kinematic parameters along the X, Y, Z directions, which are used to determine the Head Injury Criterion (HIC).

In another study published in 2020 [11], following experimental tests simulating occupant kinematics in frontal impact with a rigid barrier, the head injury severity index was evaluated for Hybrid III 5th, 50th, and 95th percentile dummies, using the same restraint system.

The results of the experimental research can be evaluated in comparison with virtual studies, as presented in study [12], where a THOR-NT dummy equipped with a standard three-point seat belt was assessed (two frontal sled tests at a speed of 40 km/h).

Another analysis comparing experimental research and numerical simulation is found in study [13], where a prototype dummy was developed and compared with a Hybrid III 50th male dummy. The comparison was carried out between the experimental sled test for the developed anthropomorphic device and the virtual study for the Hybrid III dummy.

A study from 2021 [14] extended previous research conducted by NHTSA, using the THOR-50M anthropomorphic device in frontal impact tests with a rigid barrier at a speed of 56 km/h to evaluate its performance compared to HIII-50M and NCAP test results.

1.5 Conclusions

Road accidents continue to represent a major public health problem and a significant factor of economic loss worldwide. Statistics from Romania show a high mortality rate compared to other European states, highlighting the need for stricter prevention and intervention measures. Globally, trends indicate a general decline in road fatalities over the past decades.

International standards and regulations play an essential role in promoting road safety by establishing clear and applicable requirements for modern vehicles. Vehicle safety assessment has become a complex process, and consumer information programs, such as Euro NCAP, contribute significantly to increasing public awareness.

Regarding research on vehicle-rigid barrier impact, significant progress has been made through the use of advanced anthropomorphic dummy models, such as THOR and Hybrid III, which allow for detailed analysis of occupant kinematics and interaction forces. Furthermore, the development of prototypes and sled test facilities has contributed to expanding testing capacity and improving accuracy in risk assessment. Numerical simulations offer important possibilities for optimizing vehicle construction, but the differences between experimental and simulated results highlight the need for rigorous model validation.

In conclusion, reducing the number of accidents and their consequences requires a multidimensional approach that combines strict legislative measures, innovative technologies, and effective education of traffic participants. The constant progress in vehicle safety and international regulations demonstrates that risk reduction is possible but requires sustained collective effort at both national and global levels. Continuing research into vehicle-rigid barrier interaction and integrating new technologies will significantly contribute to creating a safer road environment.

1.6 Thesis Objectives

The doctoral thesis addresses a current topic in the field of road safety, focusing on the design of technical solutions aimed at mitigating injuries to vehicle occupants in the event of frontal collisions with rigid barriers. Considering the alarming statistics on road accidents both nationally and internationally, as well

as increasingly strict regulations regarding road safety, the research objectives are directed toward contributing to the reduction of their consequences.

The main objective of the thesis is the design of a shock-absorbing system for vehicle collisions with obstacles, in order to increase occupant safety. To achieve this objective, the research includes an in-depth analysis of the current state of knowledge in the field, both from the perspective of international statistics and regulations, and from that of technological progress and existing solutions in the field of vehicle safety.

A detailed theoretical study of collisions follows, analyzing vehicle dynamics, impact attenuation systems, occupant motion kinematics, and the functioning of vehicle safety systems. The study served as a starting point for the development of the technical solution.

After completing the theoretical study, the following objectives were established:

1. Development of the mathematical model for the vehicle–rigid barrier impact.

2. Virtual study of the vehicle–rigid obstacle impact. The simulations allowed for a detailed evaluation of the interaction between the vehicle, occupants, and barrier.

3. Use of specialized equipment and software applications for experimental data acquisition and processing. The methodology applied for organizing research on physical models will allow the acquisition of a considerable volume of data, which will be used for the evaluation of injury criteria and the effects of frontal vehicle collisions with an obstacle on the occupants.

4. Design and construction of equipment for improving road safety.

5. Data recording and result analysis following research on physical models. The research aims to determine and analyze the kinematic parameters describing the behavior of the vehicle and its occupants during the collision, such as velocity and acceleration. The evaluation of injury criteria represents another aspect of the research, providing a basis for measuring the severity of injuries and the probability of their occurrence in various impact scenarios.

6. Validation of the conceived mathematical model, which will be carried out by capitalizing on the results obtained from experimental tests and those provided by numerical simulations, using statistical analysis methods that ensure the accuracy and consistency of the conclusions.

The author’s intention is to contribute to knowledge in the analysis of frontal collisions and to the foundation of an innovative technical solution for improving vehicle occupant safety.

2 THEORETICAL STUDY OF COLLISIONS

2.1 Vehicle Dynamics

2.1.1 General Equation of Vehicle Motion

For the formulation of the general equation of motion, a vehicle moving in a straight line on a road inclined longitudinally at an angle α is considered, in a transient speed regime with positive acceleration (Figure 2.1). The traction balance, which determines the dynamic equilibrium of the vehicle, can be expressed by the relation:

$$F_R = R_r + R_p + R_a + R_d \tag{2.1}$$

Where: F_R – Total wheel force; R_r – Rolling resistance; R_p – Grade resistance; R_a – Air resistance; R_d - Inertial resistance.

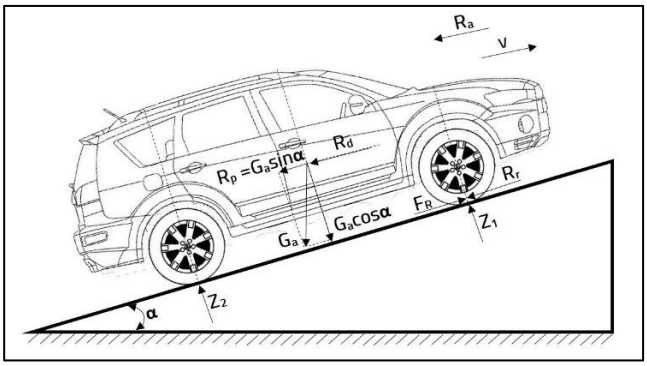

Figure 2.1 Schematic representation of the resistances to vehicle motion

The general equation of motion of the vehicle is:

$$\frac{dv}{dt} = \frac{F_R - \sum R}{\delta \cdot m_a} \tag{2.2}$$

Where: $\sum R$ - sum of all external resistances; δ - coefficient of rotating masses, v – vehicle velocity and m_a – vehicle mass [15].

2.1.2 Vehicle Collision Mechanics

A collision occurs when the momentum of the bodies changes abruptly. To develop the concept, in line with the objectives of the thesis, the rear-end collision of two vehicles is considered (Figure 2.2).

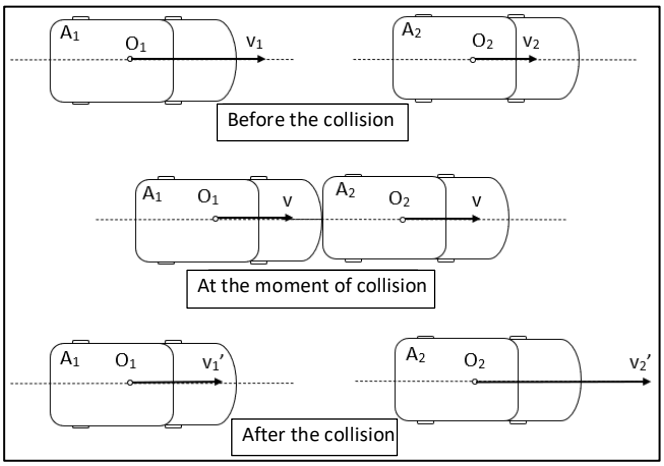

Figure 2.2 Rear-end collision between two vehicles

The vehicles denoted by A_1 and A_2 have masses m_1 and m_2, respectively. It is assumed that their initial velocities are v_1 and v_2, and after the collision they are v_1' and v_2'. Since momentum is conserved, it follows [16]:

$$H_1 - H_O = m_1 v_1' + m_2 v_2' - m_1 v_1 - m_2 v_2 \tag{2.3}$$

Before the collision, there is a compression phase, and after the collision, there is a restitution phase [17]. Depending on the coefficient of restitution (k), central collisions can be classified into three categories as follows: Elastic collisions (k=1) – During compression, kinetic energy is converted into deformation energy, which is completely restored during the restitution phase; Plastic collisions (k=0) – The bodies will only be compressed, without restitution [18], and the kinetic energy converted into deformation energy is no longer restored; Natural collisions (0<k<1) – Part of the kinetic energy converted into deformation energy during compression is restored during the restitution phase.

During a collision, the phenomenon of kinetic energy loss occurs. This loss is denoted by ΔE and can be expressed analytically as follows [19-20]:

$$\Delta E = E_0 - E_1 = \left(\frac{1}{2} \cdot m_1 v_1^2 + \frac{1}{2} \cdot m_2 v_2^2\right) - \left(\frac{1}{2} \cdot m_1 v_1'^2 + \frac{1}{2} \cdot m_2 v_2'^2\right) \tag{2.4}$$

For the particular case of a vehicle colliding with a rigid, undeformable barrier (Figure 2.3), it is considered that the barrier has infinite mass ($m_2 \to \infty$) and zero velocity both before and after the impact ($v_2 = v_2' = 0$).

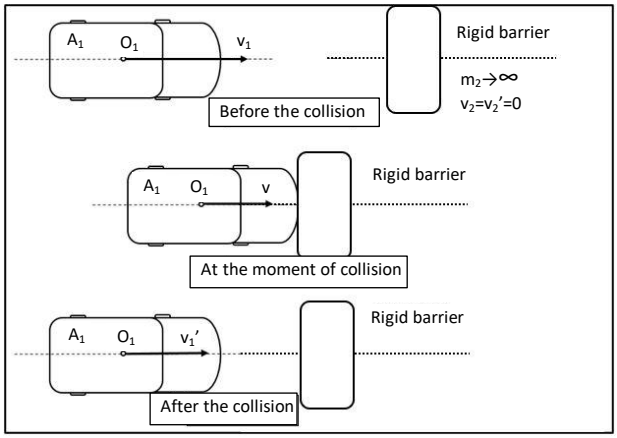

Figure 2.3 Collision between a vehicle and a rigid, undeformable barrier

The particularized form is obtained:

Initial momentum:

$$H_O = m_1 v_1 + m_2 v_2 \approx m_1 v_1 \tag{2.5}$$

Final momentum:

$$H_1 = m_1 v_1' + m_2 v_2' \approx m_1 v_1' \tag{2.6}$$

Momentum conservation (adapted):

$$m_1 v_1 \approx m_1 v_1' \Longrightarrow v_1' \approx -k \cdot v_1 \tag{2.7}$$

Where:

- $k = 0$ for plastic impact (the vehicle remains stuck to the barrier → $v_1' = 0$);
- $k = 1$ for elastic impact (the vehicle bounces back completely → $v_1' = -v_1$).

Force impulse:

$$P = m_1(v_1' - v_1) = m_1(-kv_1 - v_1) = -m_1(1+k)v_1 \quad (2.8)$$

Kinetic energy loss:

$$\Delta E = \frac{1}{2} \cdot m_1 v_1^2 - \frac{1}{2} \cdot m_1 v_1'^2 = \frac{1}{2} \cdot m_1 v_1^2 (1 - k^2) \quad (2.9)$$

2.2 Systems for Mitigating Vehicle - Obstacle Impact

2.2.1 Vehicle Structure

The bodywork of a vehicle is the upper structure used for transporting people, goods, or equipment. It can be non-load-bearing, semi-load-bearing, or load-bearing (monocoque), depending on its integration with the vehicle frame [21]. Modern monocoque bodywork models offer increased rigidity and reduced weight. The bodywork must absorb impact energy, be easy to repair, and ensure minimal aerodynamic resistance.

The structure of modern car bodies made of steel is based on the ULSAB concept (Ultra Light Steel Auto Body). This aims to optimize vehicle weight without compromising safety. Steel sheets with thicknesses of up to 1.0 mm are used for construction [over 50% high-strength low-alloy (HSLA) and ultra-high-strength (UHSLA) steels]. The low carbon content (0.05%–0.25%) in HSLA steels provides good weldability, while added alloying elements such as manganese, chromium, zirconium, titanium, etc., increase mechanical strength and durability. Figure 2.4 shows some information about the materials used in vehicle bodies.

Figure 2.4 Materials from which a vehicle body is made [22]

Current research has paved the way for the production of bodies that use carbon and glass fiber materials combined with epoxy resins. The advantage of these composite materials is metal savings, as well as simplified maintenance by replacing components with spare ones. In addition, these composites provide mechanical strength four to five times greater compared to conventional materials [22].

2.2.2 Technical Solutions for Energy-Absorbing Equipment / Components During Impact

As a result of the analysis carried out, the proposed technical solution contains a shock absorption system consisting of plastic containers (also called energy accumulators) filled with water and installed in honeycomb-type plastic supports, strategically positioned in the vehicle's front structure.

The system dimensions are: 1231 mm width, 241 mm depth, 301 mm height. It contains 45 energy accumulators.

The shock absorption system concept was designed in the Catia v5 software application and is shown in Figure 2.5.

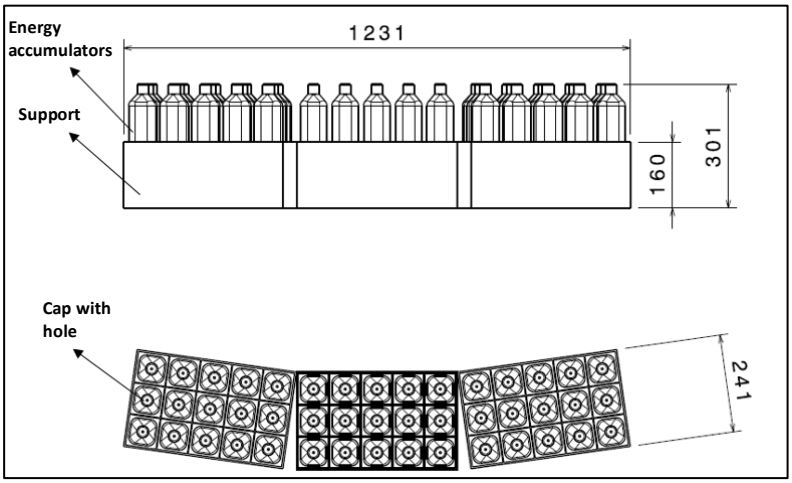

Figure 2.5 2D model of the shock absorption system formed by the set of water-filled energy accumulators (views: front, top)

The idea for this system was inspired by water-filled barriers commonly used in road construction zones [23]. These barriers provide a practical and cost-effective solution. By adjusting the size and shape of the honeycomb support or the amount of contained water, the energy absorption characteristics can be tuned for different types of vehicles and collision scenarios. In addition, water acts as a natural coolant during impact, dissipating the heat generated in the process, which could help mitigate fire hazards in certain accident scenarios. Besides the damping properties of the water-filled containers, this system offers other advantages. Firstly, using water as an impact absorption medium is environmentally friendly, as it is non-toxic. The combination of water and honeycomb-shaped plastic supports distributes impact forces evenly, reducing localized stress on the vehicle structure. This approach could be cost-effective in production due to the wide availability and low cost of both plastic materials and water, making it a viable option for mass production in vehicle safety systems.

2.2.3 Passive Safety Systems

Passive safety systems are designed to protect occupants during an accident without requiring any action from the driver or passengers. Internal passive safety includes both structural elements and safety equipment installed in the vehicle. Together, they work to reduce the forces and accelerations experienced by occupants during a collision. The structural elements absorb the impact energy and preserve survival space, while safety equipment such as airbags, seat belt assemblies, and headrests provide additional protection. In addition, these systems ensure the operability of critical components necessary for the safe evacuation of occupants after an accident [24].

Structural protection and impact energy absorption concepts that contribute to passive safety were described in subsections 2.2.1 and 2.2.2. The components of occupant restraint passive safety systems are shown in Figure 2.6.

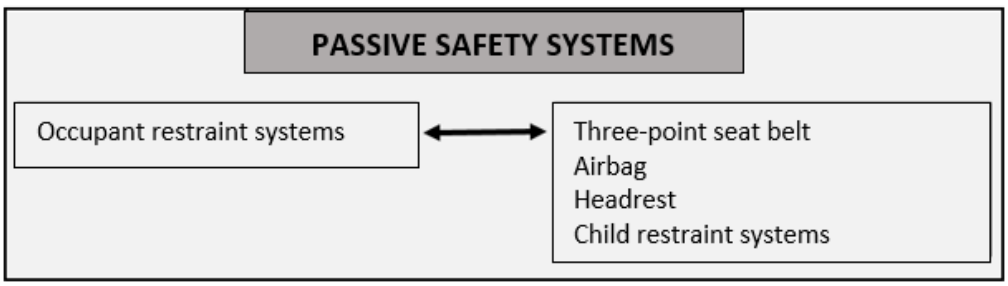

Figure 2.6 Passive Safety Systems for Occupant Restraint

2.3 Occupant Motion Kinematics Under Impact Conditions

2.3.1 Vehicle Occupants' Motion

Occupants who are not equipped with a seatbelt suffer severe injuries during frontal collisions, because they continue to move at the vehicle's pre-crash speed, followed by the sudden stop of the vehicle. This results in an impact with the interior surfaces, which provide much less protection than a seatbelt or an airbag. In contrast, seatbelts and airbags slow down the occupant's motion, reducing their speed relative to the vehicle and the impact forces [25-26].

2.3.2 Injury Criteria and Biomechanical Limits

Injury criteria and biomechanical limits are fundamental concepts in understanding human tolerance to impact. These criteria are calculated based on physical measurements that help quantify the level of force, acceleration, or stress that different parts of the body can withstand before injuries of a certain severity occur. The correlation is made using the AIS scale (Abbreviated Injury Scale) [27], which classifies injuries by severity. AIS assigns a numerical value to injuries depending on their severity, with the following scores: 1 (minor), 2 (moderate), 3 (serious), 4 (severe), 5 (critical), and 6 (fatal).

The Head Injury Criterion (HIC) is frequently used to assess the risk of injury. This criterion calculates the risk of head injury based on the resultant maximum acceleration during an impact. A high HIC value indicates a higher risk of severe head injuries such as concussion, skull fractures, or brain injuries [28]. Depending on the time interval (t_2-t_1) of 15 ms or 36 ms, the HIC is calculated using the following equation:

$$HIC = \left[\left(\frac{1}{t_2 - t_1}\int_{t_1}^{t_2} a_R(t)dt\right)^{2.5}(t_2 - t_1)\right]_{max} \quad (2.10)$$

Where: t_1, t_2 – time limits for the dt interval in which HIC reaches its maximum value (t_2-t_1 = 15 ms or 36 ms); a_R - resultant acceleration $\left(a_R = \sqrt{a_x^2 + a_y^2 + a_z^2}\right)$ measured at the dummy's head center in g.

Figure 2.7 shows the equivalence between HIC and AIS scale, established based on experiments performed on post-mortem human subjects, through frontal impact tests conducted under controlled conditions.

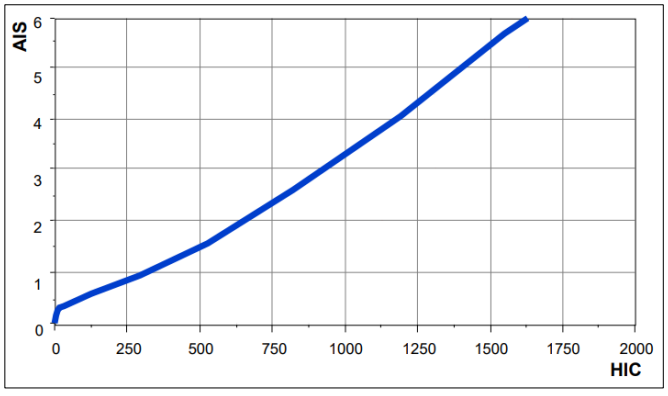

Figure 2.7 Equivalence between HIC and AIS scale [29]

One of the criteria used to evaluate the risk of thorax injury is the Thorax Acceptability Criterion (ThAC). The criterion is expressed in g units and represents the absolute maximum value of the resultant acceleration (UNECE 80 < 30 g ≈ 294.3 m/s^2/ FMVSS 208 < 60 g ≈ 588.6 m/s^2) at the thorax level over a time duration expressed in milliseconds (UNECE 80 / FMVSS 208: 3 ms).

2.4 Conclusions

In isolated systems, such as vehicle collisions, the total momentum is conserved regardless of the type of collision. However, kinetic energy is fully conserved only in elastic collisions, while in inelastic collisions, energy is transformed into heat or structural deformation.

Vehicle dynamics influence collision outcomes by affecting stability and directional control. By optimizing vehicle dynamics, manufacturers ensure the conditions to improve stability and responsiveness, which are essential for reducing accident risk and increasing road safety. Reducing aerodynamic drag improves high-speed stability and lowers fuel consumption.

Impact mitigation systems, including bodywork designs and technical solutions for equipment or components intended to absorb energy, play an essential protective role in collision scenarios. Vehicle bodies are designed with specific structural configurations, such as load-bearing, semi-load-bearing, or non-load-bearing models. Modern vehicles are built from high-strength materials, such as HSLA and UHSLA steels, to create lighter but mechanically strong structures that absorb impact energy. In addition to structural innovations, there are technical solutions for energy absorption based on advanced materials such as high-manganese-content steel, carbon fiber composites, and thermoplastics. These materials are capable of absorbing significant impact energy, protecting occupants by distributing collision forces. Moreover, the use of recyclable thermoplastics supports sustainability, offering a balance between environmental responsibility and technical performance. Passive safety systems, including crumple zones, seat belts, and airbags, are designed to activate during collisions. Occupant safety largely depends on restraint systems that control their movement during a crash. Seat belts and airbags work in tandem to reduce occupant displacement, limiting forces exerted on the head, neck, and thorax.

Injury criteria and biomechanical limits guide regulatory standards in automotive safety, setting thresholds for the forces exerted on critical body regions such as the head, neck, and thorax. Advances in biomechanics have led to sophisticated methods of predicting injury severity and to realistic crash test dummies. Research conducted with these dummies increases the accuracy of injury severity assessments and contributes to the development of automotive safety.

3 MATHEMATICAL MODELING AND NUMERICAL SIMULATIONS OF VEHICLE - RIGID BARRIER IMPACT

3.1 Development and Implementation of the Mathematical Model

3.1.1 Basic Concepts of Impact Kinematics

In the event of an accident, the occupant's kinematics is described by three distinct phases of motion:

1. The beginning of the occupant's motion from the resting position on the vehicle seat until their initial impact with the interior components of the cabin;

2. From the impact of the occupant with the vehicle components until the occupant's acceleration;

3. From the beginning of the occupant's accelerated motion until its end [25].

3.1.2 Reference Mathematical Models for Frontal Impact

The mathematical modeling of the vehicle–rigid barrier impact is based on a simplified model consisting of a mass and an elastic spring. The system allows the vehicle to move along the X direction toward a rigid barrier, the model being characterized by a single degree of freedom. The car body structure has special zones for shock energy absorption, so the model can be optimized by mounting a damper at the front part [30].

3.1.3 Input and Output Parameters

The input parameters are static and represent the initial conditions of the model, and their values are constant and therefore do not vary over time. They are: m_1- vehicle mass; m_2- occupant's thorax mass; m_3- occupant's head mass; k_1- stiffness of the vehicle's front part; k_2- stiffness of the restraint system; k_3- stiffness of the occupant's neck; c_1- damping coefficient for the vehicle's front part; c_2- damping coefficient for the restraint system; c_3- damping coefficient for the occupant's neck; F- force transmitting the motion of the system.

The output parameters are dynamic, and their values vary over time. By differentiating with respect to time, the velocity and acceleration values of the vehicle, as well as of the occupant's head and thorax, are determined: $v_1(\dot{x}_1), a_1(\ddot{x}_1)$- vehicle velocity and acceleration; $v_2(\dot{x}_2), a_2(\ddot{x}_2)$- occupant's thorax velocity and acceleration; $v_3(\dot{x}_3), a_3(\ddot{x}_3)$- occupant's head velocity and acceleration.

3.1.4 Adopted Working Assumptions

The mathematical model uses a system composed of three distinct masses, which are associated with the vehicle (m_1), the occupant's thorax, and head (m_2 and m_3 respectively).

The connections between the masses of the system, as well as between the vehicle and the rigid barrier, are made using elastic springs with different stiffnesses. To dissipate part of the energy released by the springs associated with bodies m_1, m_2, and m_3 and to reduce the number and amplitude of oscillations, dampers are installed. The damping coefficients (c) are determined analytically, as follows:

$$c_c = 2\sqrt{m \cdot k} \tag{3.1}$$

$$c = \zeta \cdot c_c \tag{3.2}$$

Where: c_c - the coefficient of critical damping; ζ - the fraction of critical damping.

Systems with critical damping, which return to the initial state in the shortest possible time, correspond to a fraction of critical damping value ζ=1. When ζ >1, a higher damping effect occurs and the system

becomes overdamped. The system becomes underdamped when the condition $\zeta < 1$ is met. The value of the fraction of critical damping is determined experimentally.

It is considered that the deformation force is proportional to the spring stiffness, so the simulation of vehicle deformation is carried out through an elastic element, ensuring stiffness k_1 between the deformable front part of the vehicle and the rigid barrier. The occupant is restrained in the seat by a seatbelt, represented by an elastic spring with stiffness k_2. The neck joint is simulated by the elastic element between the head and thorax, having stiffness k_3. Using Hooke's law, the stiffness values of the three springs can be calculated by the ratio between the applied force F_A and the resulting deformation x:

$$k = \frac{F_A}{x} \tag{3.3}$$

The model is characterized by three degrees of freedom corresponding to the three masses performing translations along the x-axis. Displacements x_1, x_2, and x_3 are allowed, corresponding to the vehicle, the thorax, and the head of the occupant, respectively. The displacements satisfy the condition $x_3 > x_2 > x_1$.

The motion equations of the system are determined by drawing the free-body displacement diagram for each mass and then applying Newton's second law of motion (force = mass * acceleration along the X-axis) to obtain the system of differential equations.

The mathematical model has the following limitations:

-It only allows translations along the X-axis. The model is characterized by three degrees of freedom.

-The model calculates only the kinematic parameters of the occupant's head and thorax.

3.1.5 Development of the Calculation Flow Diagram

Figure 3.1 shows the calculation flow diagram, illustrating the essential stages of the mathematical model development.

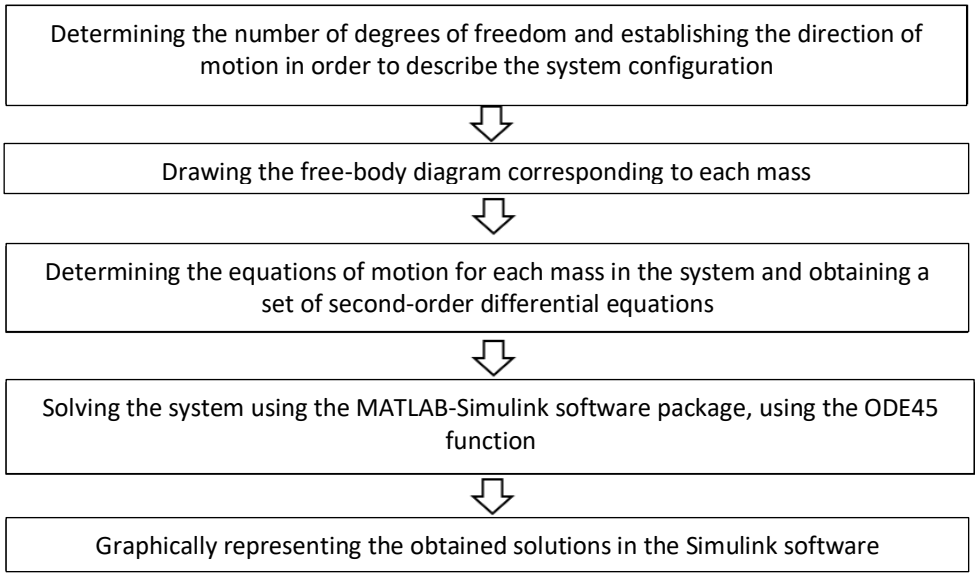

Figure 3.1 Calculation flow diagram

3.1.6 Graphical Representation of the Mathematical Model

For the elaboration of the mathematical model, necessary for the numerical simulation of the dynamics of the vehicle and the occupant, in the case of a frontal impact with a rigid barrier, a scheme of the mass-spring-damper system with three degrees of freedom was created (Figure 3.2).

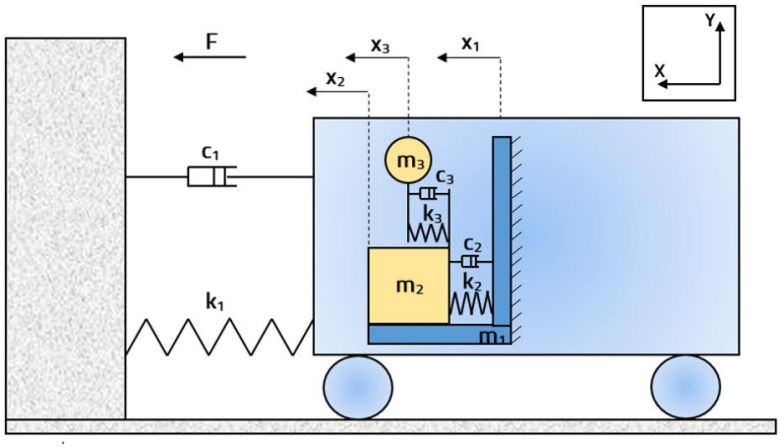

Figure 3.2 Mass-spring-damper system with three degrees of freedom

3.1.7 Determination and Implementation of the Equations in the Calculation Flow Diagram

The system is characterized by three degrees of freedom and therefore three equations of motion corresponding to the displacements of the three bodies along the X axis will be determined.

Knowing that for systems with translational motion, the sum of the external forces acting on a body in a given direction is equal to the product of its mass and acceleration in that direction, the calculation relations for the equations of motion will be established by applying Newton's second law of mechanics.

The positive direction $\left(\overset{+}{\Leftarrow}\right)$ is chosen according to the direction of movement, after which the equations describing the motion of the bodies that make up the system are determined.

For body m_1:

$$F - c_1\dot{x}_1 - c_2(\dot{x}_1 - \dot{x}_2) - k_1x_1 - k_2(x_1 - x_2) = m_1\ddot{x}_1 \tag{3.4}$$

For body m_2:

$$-c_2(\dot{x}_2 - \dot{x}_1) - c_3(\dot{x}_2 - \dot{x}_3) - k_2(x_2 - x_1) - k_3(x_2 - x_3) = m_2\ddot{x}_2 \tag{3.5}$$

For body m_3:

$$-c_3(\dot{x}_3 - \dot{x}_2) - k_3(x_3 - x_2) = m_3\ddot{x}_3 \tag{3.6}$$

The system of three second-order differential equations can be solved in MATLAB-Simulink.

3.1.8 MATLAB-Simulink Software Interface

The MATLAB software application is used in a variety of engineering fields, as well as in various scientific computing applications. The MATLAB package has a module called Simulink, which is an integrated graphical programming application. Simulink is used for modeling, analysis, and simulation of dynamic systems, as well as for control algorithms. The Simulink module has its own library of blocks and subsystems, with the possibility of combining discrete and continuous systems.

The types of blocks can vary, depending on the user's preferences regarding mathematical modeling in accidentology. Thus, forces are introduced through "Constant" blocks. For arithmetic operations, "Add" blocks are used, for multiplication by a constant value, "Gain" blocks are used, for integrating an input signal with respect to time with the result as the output signal, "Integrator" blocks are used, and for the graphical representation of solutions, "Scope" blocks are required.

Many modeling problems, with engineering applications, can be formulated using ordinary differential equations (ODE). The Simulink package has a predefined calculation module to solve ODEs (e.g., ODE45 – Dormand-Prince, ODE15s – stiff/NDS, etc.) [31-32].

In conclusion, after choosing the solver, the simulation duration is set and the simulation is run. The "Scope" block displays time-domain signals.

3.1.9 Working Procedures and Model Implementation

The equations of motion were solved using the Simulink-MATLAB package, and blocks from the application library were used for modeling.

Thus, input parameters were calculated for a vehicle with mass m_1 of 1020 kg, as well as for the Hybrid III 50^{TH} male dummy with a total mass of 77.7 kg, having a thorax mass m_2 of 40.23 kg, and a head mass m_3 of 4.54 kg.

The numerical simulation was carried out for an initial vehicle velocity of 16.7 m/s.

The input force to the system was calculated by multiplying the masses of the system components by the acceleration. Thus, the absolute value of the maximum vehicle deceleration of 255 m/s² was considered, this value being taken from the experiment carried out by the author at the Research and Development Institute of Transilvania University of Brasov for the impact of the vehicle with a rigid barrier at a velocity of approximately 16.7 m/s. The force was calculated based on the total mass of the system, including both the vehicle and the complete mass of the occupant. From the same experiment, the average deformation value in the frontal part (0.372 m) was taken, necessary for determining the vehicle stiffness (k_1) [33].

The determination of stiffness k_2 and k_3 was carried out using experimental displacement data from specialized scientific publications [34-35]. The stiffness of the restraint system was calculated for a force applied at the thorax level of 7000 N, resulting in a thorax deformation of 0.043 m. The neck stiffness was determined for a force applied of 4200 N and a deformation of 0.107 m, which represents the average neck length of a human of 0.1 m and its actual deformation of 0.007 m.

The damping coefficients [N*s/m] were calculated for a fraction of the critical damping of 0.3. The value is determined experimentally for better accuracy of the results.

In Figure 3.3, the input parameters used for modeling the system are presented.

parametri_intrare.m

```
1   m1=1020;
2   m2=40.23;
3   m3=4.54;
4   F=279913.5;
5   k1=699193.5;
6   k2=162790.7;
7   k3=39252.3;
8   c1=16023.2;
9   c2=1535.5;
10  c3=253.3;
11
```

Figure 3.3 Input parameters for mathematical modeling

The three equations of motion were modeled in Simulink by connecting "Constant" blocks for the system force, "Gain" blocks for multiplying stiffness and damping values, "Add" blocks for setting the addition or subtraction signs (+/-), and "Integrator" blocks for time integration.

The results were displayed using "Scope" blocks, with two blocks having three inputs each for the graphical representation of system velocities (x1', x2', x3') and accelerations (x1'', x2'', x3'').

The model is presented in Figure 3.4.

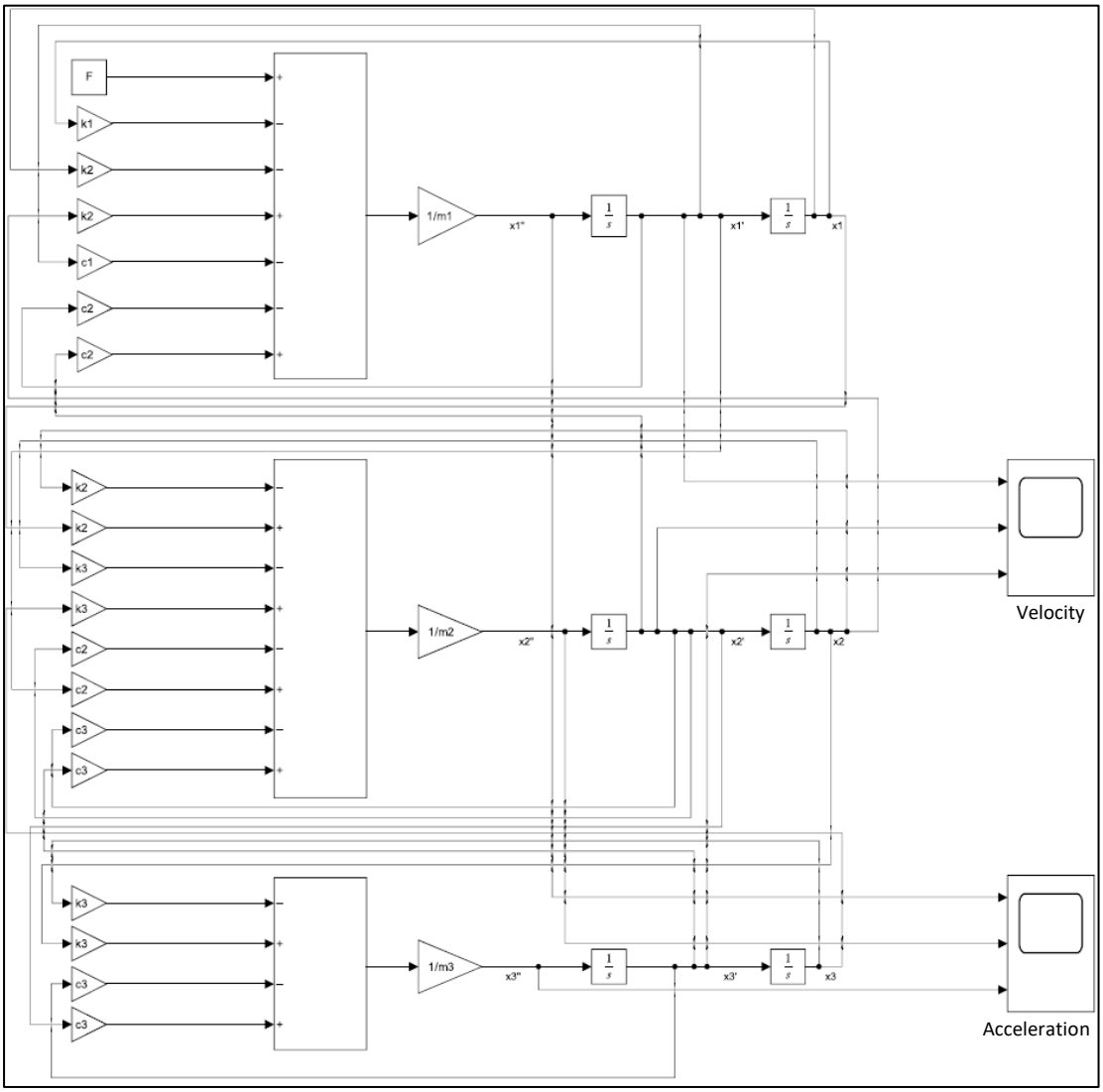

Figure 3.4 Model for vehicle impact with a rigid barrier

The system was solved using the ODE45 solver for a simulation duration of 0.3 seconds (Figures 3.5–3.6).

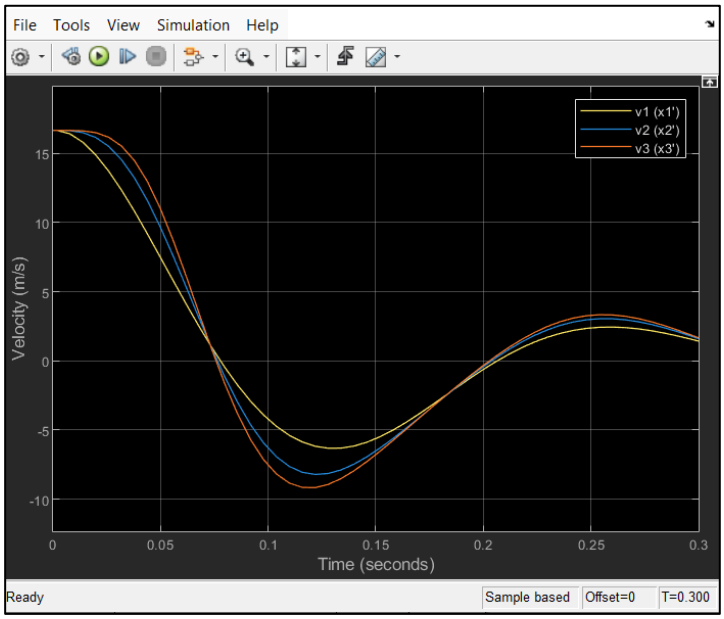

Figure 3.5 System velocities

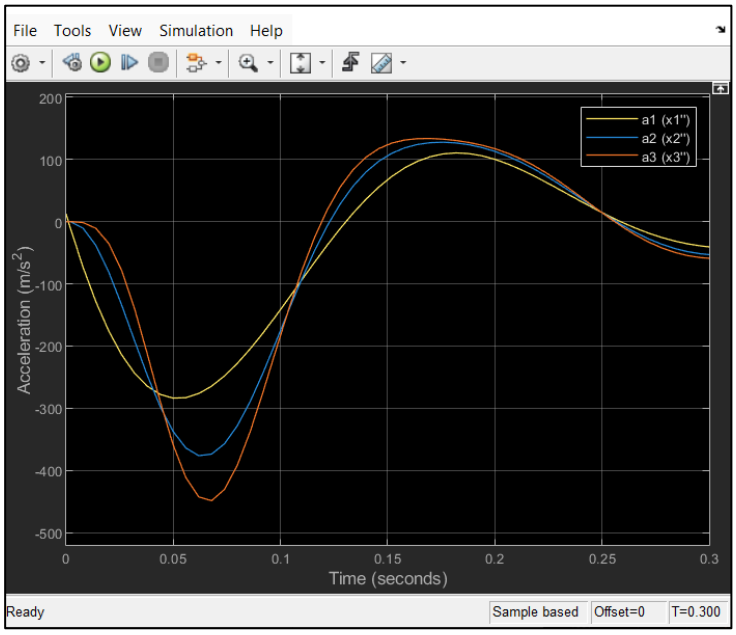

Figure 3.6 System accelerations

Before the impact, all three components of the system (vehicle, thorax, head) have the same velocity of 16.7 m/s. During the collision, the deceleration of the vehicle is observed, followed by the delayed responses of the occupant's thorax and head. The absolute values of the maximum deceleration are: $|a_1|$max - vehicle (283,7 m/s²), $|a_2|$max - thorax (376,2 m/s²), $|a_3|$max - head (448,6 m/s²).

3.2 Advanced Analytical Methods for Extending Mathematical Modeling Toward Finite Element Analysis

In the context of extending previous mathematical modeling, the finite element method (FEM) is used to meet the increasingly strict requirements of modern engineering. FEM facilitates the transition from simplified approaches to a detailed description of the behavior of systems with multiple degrees of freedom.

3.2.1 Lagrange Equations

The classical analytical expression of Lagrange equations is as follows:

$$\frac{d}{dt}\left\{\frac{\partial L}{\partial \dot{\delta}}\right\}_L - \left\{\frac{\partial L}{\partial \delta}\right\}_L = 0 \tag{3.7}$$

Where: L – the Lagrangian; δ – the generalized coordinates; $\dot{\delta}$ - the first-order derivative of the generalized coordinates.

The method based on Lagrange equations involves performing three different differentiations $\left(\left\{\frac{\partial L}{\partial \dot{\delta}}\right\}_L ; \frac{d}{dt}\left\{\frac{\partial L}{\partial \dot{\delta}}\right\}_L ; \left\{\frac{\partial L}{\partial \delta}\right\}_L\right)$.

3.2.2 Gibbs-Appell Equations

Within analytical mechanics, the Gibbs-Appell equations constitute an alternative method to mathematical modeling with Lagrange equations. The application of this method requires knowledge of the energy of accelerations E_a. The expression describing the Gibbs-Appell equations is as follows:

$$\frac{\partial E_a}{\partial \ddot{q}_j} = Q_j \tag{3.8}$$

Where: $\ddot{q}_j$- the second derivative of the generalized coordinates, and $j = \overline{1,n}$; Q_j- the generalized forces, and $j = \overline{1,n}$.

Unlike the Lagrange method, the Gibbs-Appell method involves a smaller number of differentiations, which leads to a reduction in the amount of required calculations. This characteristic becomes essential in the context of finite element models, which involve a significant number of degrees of freedom and, implicitly, a large number of operations. The reduction in the number of calculations provided by the Gibbs-Appell method can have a considerable impact on optimizing computational processing time [36-38].

3.3 Finite Element Analysis of Vehicle - Rigid Barrier Impact

The finite element model for simulating the frontal impact between a vehicle and a rigid barrier was created in the Hypermesh application from the Altair Hyperworks suite. The analysis was performed using the RADIOSS solver integrated in the same package. The post-processing of data was carried out using the Hyperview and Hypergraph applications.

The vehicle model adopted for the impact study includes a front shock absorption system. This system consists of a set of water-based energy accumulators and was modeled to be equivalent to the one that will be used in the experimental test. In the finite element analysis, a configuration with 27 energy accumulators is used, while in the experimental test, the shock absorption system will contain 45 accumulators. The finite element model contains 117,800 nodes and 123,600 elements (Figure 3.7).

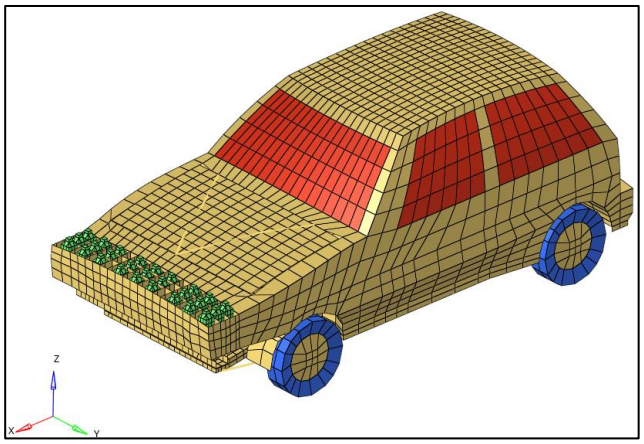

Figure 3.7 Discretized model of the vehicle equipped with a front damping system

The types of elements used are SHELL-type with three or four corner nodes, each node having six nodal degrees of freedom. The coding of these element types in the software application is: SHELL3N for triangular SHELL elements and SHELL4N for quadrilateral ones. Other types of elements used were solid HEXA elements with eight corner nodes, coded HEXA8N. These were used for discretizing the engine components, radiator, and wheel rims. 1D (uniaxial) elements were mainly used for steering and suspension components, as well as for simplified modeling of the front and rear axles.

In Figure 3.8 the materials used in the impact analysis are presented, differentiated by identification code (ID) and a distinct color:

Materials	ID	Include	Defined	Type	Card Image
windshield	1	0	☑	ELASTO-PLASTIC	M2_PLAS_JOHNS_ZERIL
rubber	2	0	☑	ELASTO-PLASTIC	M2_PLAS_JOHNS_ZERIL
steel	3	0	☑	ELASTO-PLASTIC	M2_PLAS_JOHNS_ZERIL
Plastic_bottle	5	0	☑	ELASTO-PLASTIC	M27_PLAS_BRIT
water	6	0	☑	HYDRODYNAMIC	MLAW6

Figure 3.8 Materials used in the finite element analysis

The material properties are presented in the thesis.

In Figure 3.9 the numbering of the points on the front structure can be seen, where the kinematic parameters (displacement and velocity) were recorded in the impact direction.

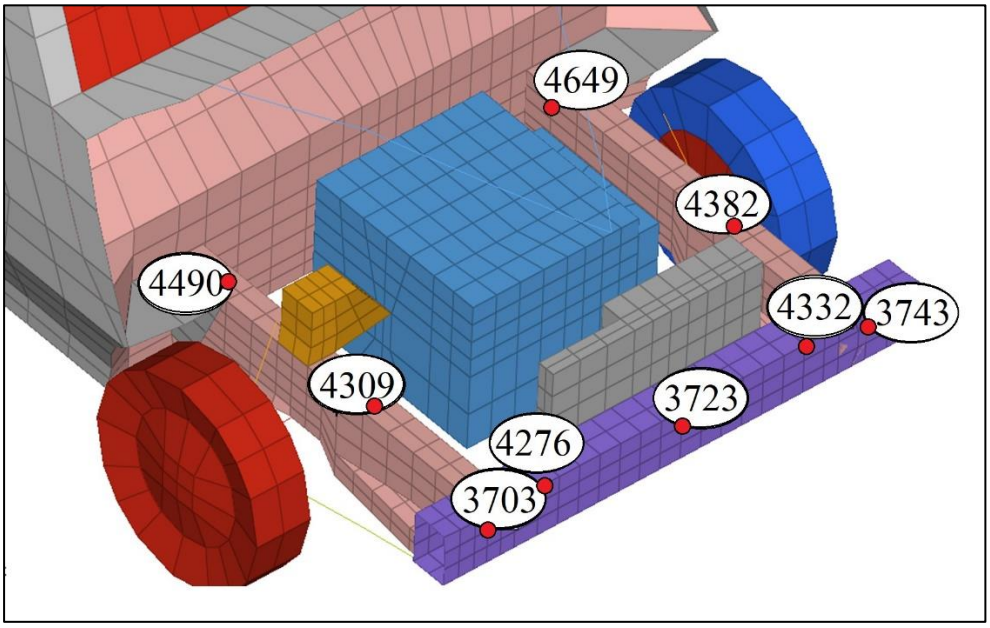

Figure 3.9 Numbering of points on the front structure for reading kinematic parameters

The simulation was performed in the transient domain, considering that the impact scenario takes place over a very short time interval of approximately 60 ms. The impact velocity used in the analysis scenario was considered to be equal to the initial velocity that will be used in the experiment (42 km/h). The object with which the vehicle collided was considered rigid, without elasticity properties. The analysis is theoretical and does not represent a real case.

Based on the analyses carried out, the following results were obtained and are presented in graphical form. Figure 3.10 illustrates the time evolution of internal energy and kinetic energy during the frontal impact.

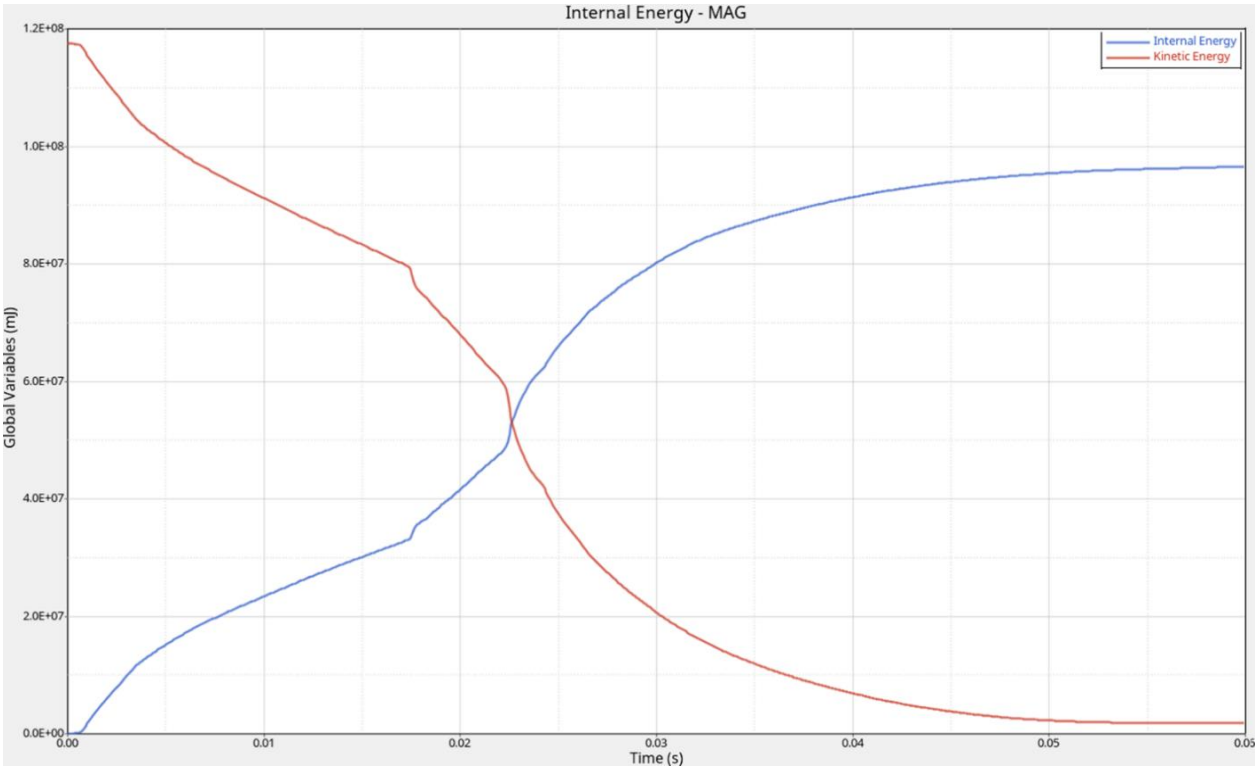

Figure 3.10 Time evolution of internal energy and kinetic energy

Figures 3.11–3.12 show the evolution of displacement and the variation of velocity at the points chosen on the front structure.

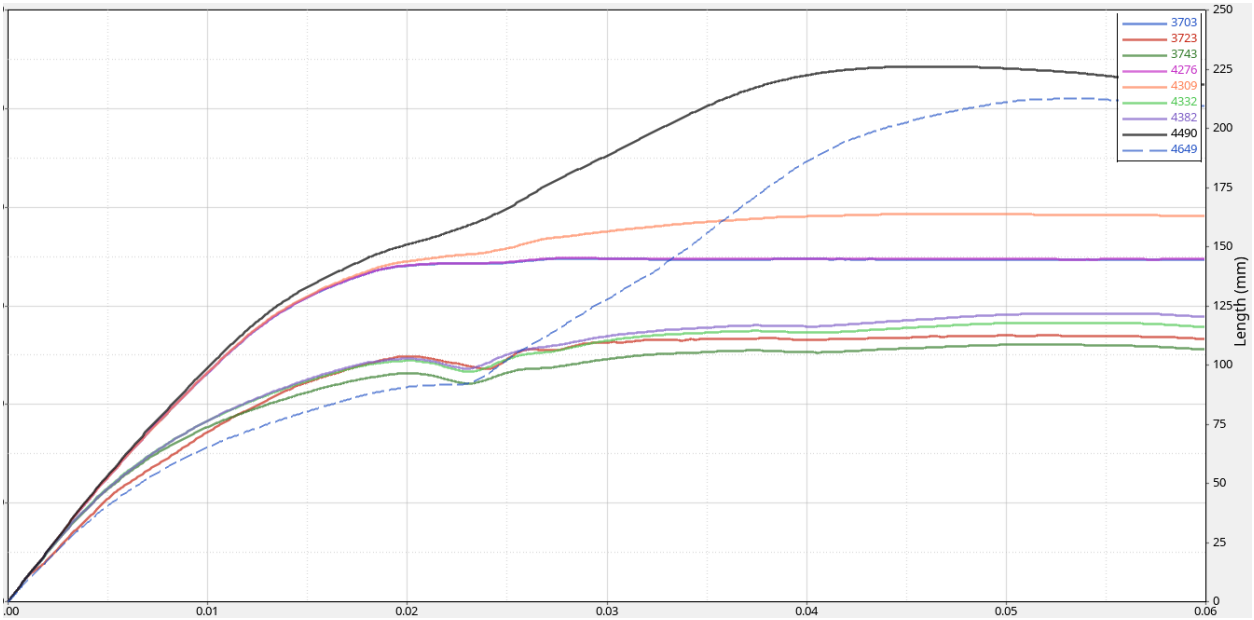

Figure 3.11 Time variation of displacement for selected nodes

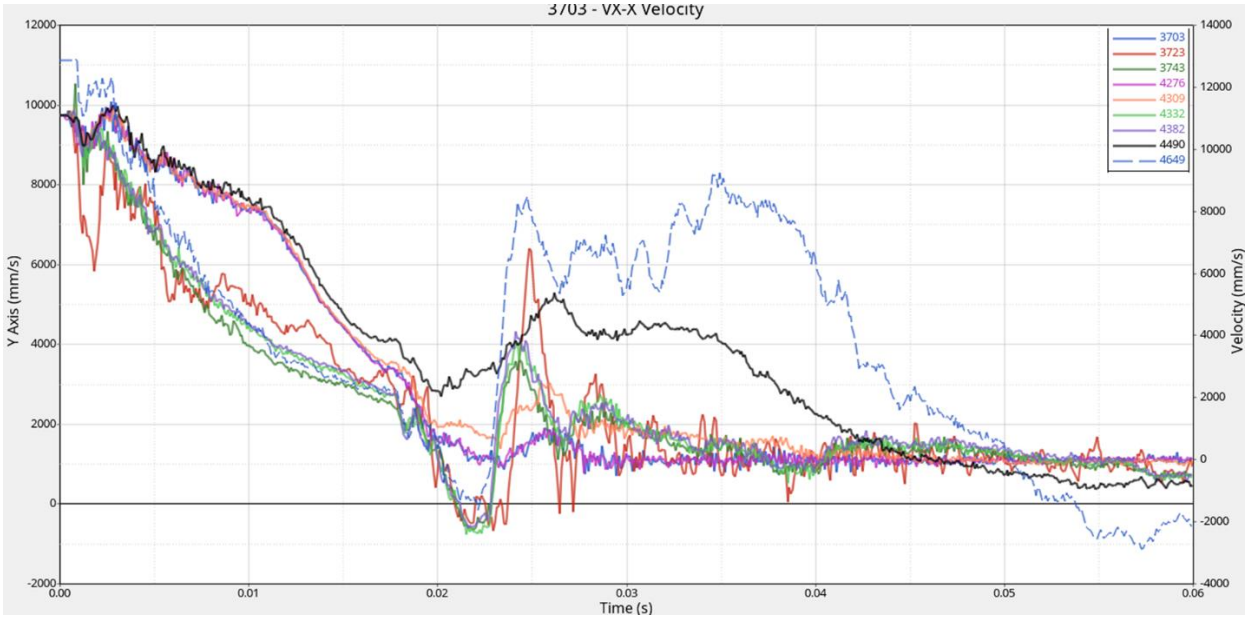

Figure 3.12 Time variation of velocity for selected nodes

3.4 Evaluation of Prediction Errors in Mathematical Models

MAPE (Mean Absolute Percentage Error) is a method frequently used to evaluate the accuracy of a mathematical model by comparing simulated values with measured ones. It expresses the error as a percentage, providing an intuitive and comparable measure of the average deviation between the simulated results and the experimental data. The formula for calculating MAPE is:

$$MAPE = \frac{1}{n}\sum_{i=1}^{n}\left|\frac{y_{measured,i} - y_{simulated,i}}{y_{measured,i}}\right| \cdot 100 \quad (3.9)$$

Where: $y_{measured}$ - represents the experimental values; $y_{simulated}$ - are the calculated values; n - is the total number of points.

This method will be used for validating the mathematical model.

3.5 Conclusions

This chapter presented the reference mathematical models used to study the impact between a vehicle and a rigid barrier.

The basic mathematical models were adapted for the development of a model of the frontal impact between the vehicle and the rigid barrier, taking into account the occupant. A system of masses, springs, and dampers was used to create the model, and the input and output parameters, as well as the working hypotheses, were defined. The model configuration did not include an energy-absorbing system for the vehicle impact. Subsequently, based on a calculation flowchart, equations that can be solved in specific software applications were determined and implemented. The system of equations was solved using the Matlab-Simulink package with the ODE45 solver. The impact simulation was carried out at a speed of 60 km/h. The results displayed by Simulink are illustrated through representative graphs of the displacements, velocities, and accelerations of the vehicle and the occupant. All components (vehicle, thorax, head) had an initial speed of 16.7 m/s. During the collision, the maximum decelerations were recorded: −283.7 m/s² for the vehicle, −376.2 m/s² for the thorax, and −448.6 m/s² for the head. The time evolution of the kinematic parameter curves highlights a delayed response of the occupant's components (head, thorax) compared to the vehicle, as a result of the progressive transmission of impact forces.

The mathematical model will be subsequently validated, in a separate chapter, using the MAPE method.

Advanced analytical methods were studied in order to extend the mathematical modeling towards finite element analysis. The energy of accelerations forms the basis of modern analytical formulations, such as the Gibbs-Appell method. Integrating this quantity into the description of multibody system (MBS) dynamics provides a distinct perspective compared to traditional approaches, such as Lagrange equations.

Compared to Lagrange equations, the Gibbs-Appell method stands out due to the reduced number of differentiations required, which leads to a significant decrease in computational load. This feature becomes particularly important in complex problems where computational efficiency is essential.

Both methods, Lagrange and Gibbs-Appell, find applicability in specific contexts. Lagrange equations are more familiar and widely used due to their intuitive formulation based on kinetic and potential energy. In contrast, the Gibbs-Appell method, although less commonly used, offers advantages in problems that require a large volume of calculations due to its more compact formulation.

The analytical methods studied contribute to the extension of the initial mathematical model, facilitating the transition to advanced analysis methods, such as finite element analysis. For this purpose, the vehicle was modeled with a shock absorption system (27 energy accumulators), but without including the occupant. The simulation of the vehicle–rigid barrier impact was performed at a velocity of 42 km/h. The finite element analysis of the impact demonstrated that the vehicle structure is capable of dissipating the collision energy through controlled deformations, especially in the front area. The initial kinetic energy of the system was 1.18×10^8 mJ, and during the collision, a reduction of this energy was observed, correlated with an increase in internal energy. After 0.022 s, the values of the two forms of energy became equal, and at 0.06 s the internal energy reached its maximum value of 0.97×10^8 mJ, while the kinetic energy became negligible. The maximum deformation recorded in the front area was 415.5 mm. In the selected nodes, displacements varied between 105 mm and 227 mm. The maximum recorded speed was 11.1 m/s, and the absolute minimum speed was 2.8 m/s, in the same node. The results obtained can be used to improve structural behavior, with a focus on optimizing energy-absorbing components. Thus, the study contributes to the foundation of more efficient technical solutions for increasing safety in the event of frontal collisions.

4 SOFTWARE APPLICATIONS, EQUIPMENT, AND PROCEDURES USED FOR THE ACQUISITION AND PROCESSING OF EXPERIMENTAL DATA

This chapter presents the equipment, software applications, and procedures used for the acquisition and processing of data for the experiments to be carried out. The measured kinematic parameters are velocity and acceleration for the vehicle and dummies (head and thorax). The choice of instruments, together with the procedures used, allows the data to be used to achieve the proposed objectives..

4.1 Equipment Used for Experimental Data Acquisition

The equipment that will be used in the experimental research:

1. PicDAQ4 – data acquisition platform for measuring vehicle accelerations;

2. PicDAQ5 – data acquisition platform for measuring dummy head and thorax accelerations.

4.1.1 Measurement of Velocity Using GPS Systems

The vehicle velocity can be evaluated using the GPS system. The hardware components that make up the GPS system are a Venus GPS device, the ANT-555 antenna, and a laptop.

The GPS system provides accurate position and speed data. It can be used for vehicle navigation systems, automatic location systems, or for various interactions with other types of equipment. The GPS receiver (Venus 638FLPx-L) uses the ANT-555 antenna, and the electronic unit converts the electrical signal picked up from the antenna into data (binary or text). The data received from the GPS system are represented in the form of NMEA codes [39].

4.1.2 Measurement of Accelerations at Vehicle and Occupant Level - PiqDAQ, CDL

The PicDAQ systems are data acquisition platforms used for recording dynamic data, by means of which accelerations and angular velocities can be measured. The platforms are developed by the Austrian company DSD and are intended for impact, braking, or maneuverability tests.

Figure 4.1 shows the PicDAQ 5 data acquisition platform. It can be used to record dummy head and thorax accelerations.

Figure 4.1 Data acquisition platform – PicDAQ 5

Multiple analog input channels are necessary to cover a wide range of uses, such as measuring the steering wheel angle, wheel speed, etc. The characteristics of collision simulation tests as well as braking tests are evaluated using two tri-axial accelerometers (in the ranges ±1.5 g ≈ ±14.7 m/s² and ±200 g ≈ ±1962 m/s²), and roll, pitch, and yaw movements are measured using a tri-axial angular velocity sensor (in the range ±300 degrees/second).

Figure 4.2 shows the PicDAQ 5 system installed inside the dummy's thorax.

Figure 4.2 Installation location of the PicDAQ 5 system

Another data acquisition platform includes the PicDAQ 4 accelerometer (Figure 4.3). It can be used to record vehicle accelerations.

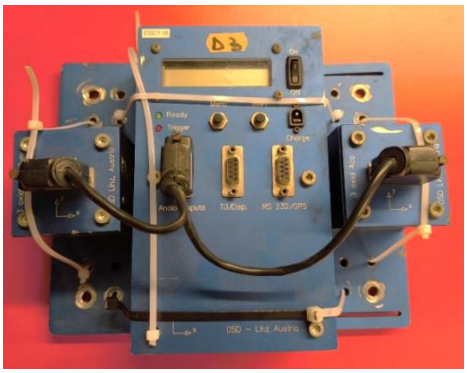

Figure 4.3 Data acquisition platform – PicDAQ 4

The equipment consists of the main control unit and two sensor blocks. The main unit contains the control buttons, display, and connectors. One of the blocks includes three axial acceleration sensors used for the 5 g range (49.1 m/s²) as well as three angular velocity sensors (150°/second). The other block includes three axial acceleration sensors for high values up to 50 g (490.5 m/s²). For maneuverability and braking tests, the angular velocity sensors and the 5 g (49.1 m/s²) acceleration sensors are used, while for impact tests the sensors with the limit up to 50 g (490.5 m/s²) are used. Figure 4.4 shows the installation of the PicDAQ 4 accelerometer inside the vehicle.

Figure 4.4 Installation location of the PicDAQ 4 system

Calibration and verification of the accelerometers involves comparing the recorded values with gravitational acceleration g. This method involves measuring acceleration at angles of 0° and 180°, for

values of 1 g and -1 g respectively. Conversion from g to m/s² is also performed. Measurements must be carried out on all three axes (X, Y, and Z) to ensure complete calibration.

The data recording platforms do not require additional power supply, so the accelerometers have no extra cables. Both acquisition platforms have a dedicated software application called PocketDAQAnalyzer through which the obtained data can be acquired, analyzed, and processed [40].

The CDL system was developed based on MEMS accelerometers and is used for data acquisition in the field of accidentology.

The CDL system uses the ADXL 337 sensor to measure accelerations (-3 g ≈ -29.4 m/s² and +3 g ≈ +29.4 m/s²), and the ADXL 377 sensor to measure high accelerations (-200 g ≈ -1962 m/s² and +200 g ≈ +1962 m/s²). Both sensors are analog, developed by Analog Devices, and data can be recorded on the X, Y, and Z axes [41].

4.2 Software Applications for Experimental Data Processing

The software applications for data processing, which will be used in experimental research, are the following:

1. Tracker – velocity parameters for vehicles and dummies (head, thorax);

2. PocketDaqAnalyzer - vehicle and dummy accelerations (head, thorax).

4.2.1 Processing of Velocity Parameters

The processing of the velocity parameters obtained with the GPS system is carried out using the DS-5 software application. The use of the application is based on data acquisition in the form of ASCII (text) files. The sequences are interpreted by the user who collects the necessary information such as longitude, latitude, speed, date, navigating to the section where the recorded data are displayed or directly from the NMEA sequence. By recording the longitude and latitude at different time intervals (distance traveled), speed can be calculated [39].

For displaying and processing the velocity parameters based on the NMEA sequences, the GPS-NMEA Processor software application can be used.

4.2.2 Processing of Acceleration Data

The files recorded with the PicDAQ systems are processed with the PocketDaqAnalyzer software application.

After selecting the data loading mode (automatic), the option corresponding to the platform and sensor orientation is chosen. Next, “CRASHTEST” is activated for accidentology tests. In the application's graphical window, there is also the “BRAKETEST” option, which represents braking tests. The specific characteristic of these two options is that the first uses accelerometers that measure high accelerations, while the second option uses accelerometers for measuring low accelerations. To ensure data accuracy, a period is set for automatic correction of the bias between the sensor output signal and the reference value (the mean of the measured values).

The acceleration data of the dummy's head, positioned in the driver’s seat, were recorded with the PicDAQ 5 system. The experiment was carried out by the author at the Research and Development Institute of Transilvania University of Brasov, to simulate the frontal impact of a vehicle with a rigid barrier at a speed of 31 km/h.

The channels used for recording the accelerations were Aux1, Aux2, and Aux3 corresponding to the three axes (X, Y, and Z). CFC (Channel Frequency Class) is a parameter used in signal processing to filter the data

recorded by the accelerometers. In the case of the dummy's head, during the acquisition of acceleration data, the applied filter is CFC1000. The filter selection is made according to the SAE J211 standard.

Figure 4.5 shows an example of a graph obtained after data acquisition by the sensor. For a detailed visualization, the acceleration graph (measured in g) is trimmed to an interval of interest. After successive processing, the dependency graph is obtained.

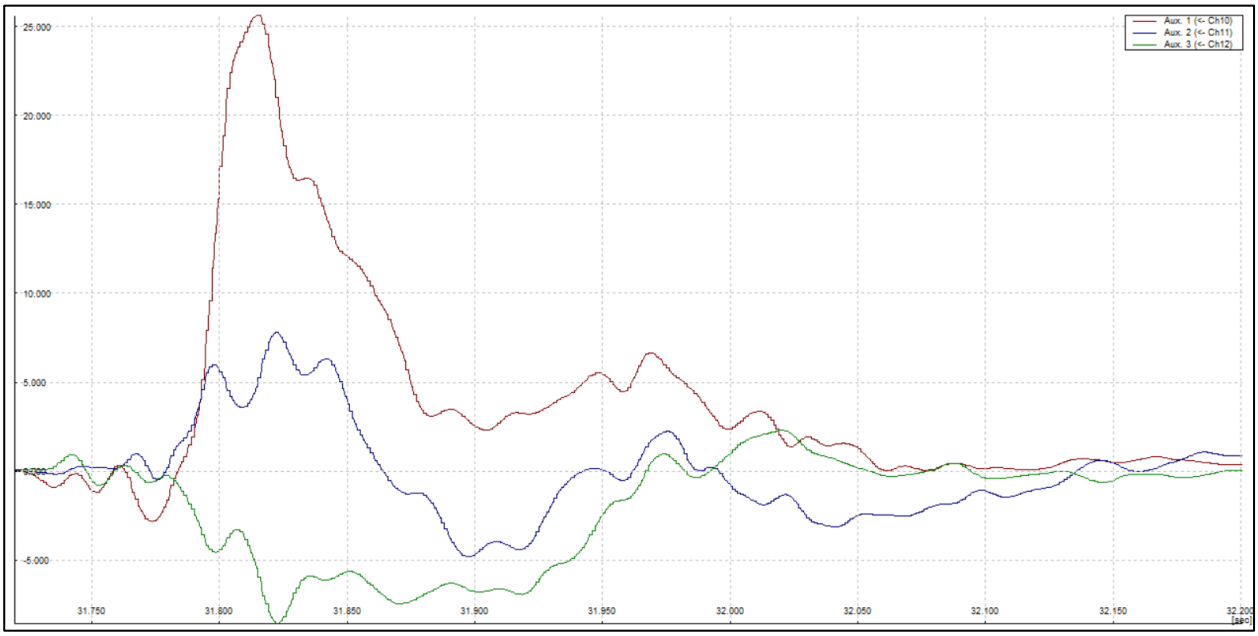

Figure 4.5 Enlarged view of the trimmed graph section

The maximum acceleration on the X-axis is 25.6 g (251.1 m/s²), indicating the main direction of impact. On the Y-axis, the maximum acceleration is 7.8 g (76.5 m/s²), and on the Z-axis, the absolute value of the maximum deceleration is 8.5 g (83.4 m/s²). The data processed with PocketDAQAnalyzer can also be exported and graphically represented later in Microsoft Excel.

For viewing and preliminary processing of the data, the Accele software application can also be used. The application is developed to read and process the data recorded by the CDL accelerometer.

4.2.3 Processing of Video Samples - Tracker

Tracker is a free video analysis tool developed on the Java Open Source Physics platform [42].

Video sample processing and display of kinematic parameters (displacement, velocity, and acceleration) can be done through the Tracker software application. Video samples filmed with a high-speed camera are used.

A video sample (600 frames per second) is to be processed to determine the velocity parameter at the level of the dummy's head, installed in the vehicle. The experiment, carried out by the author at the Research and Development Institute of Transilvania University of Brasov, consisted in simulating the frontal impact of a vehicle with a rigid barrier.

After choosing the interval in which the application will collect data, the axis system and the calibration ruler length are set for the measurements to be made relative to a global system. The measurements are made using the mass points of the analyzed bodies. Mass points refer to the concept of mass being concentrated at a single point. These will be fixed on the markers applied to the bodies before performing the experiment. When the bodies move, the points will follow the movement of the marks applied to the vehicle, thorax, and head of the occupant.

Finally, the parameters (displacement, velocity, acceleration) will be obtained after performing the video analysis. Figure 4.6 shows an example of the velocity parameter graph of the occupant's head, on the X-axis, displayed in Tracker:

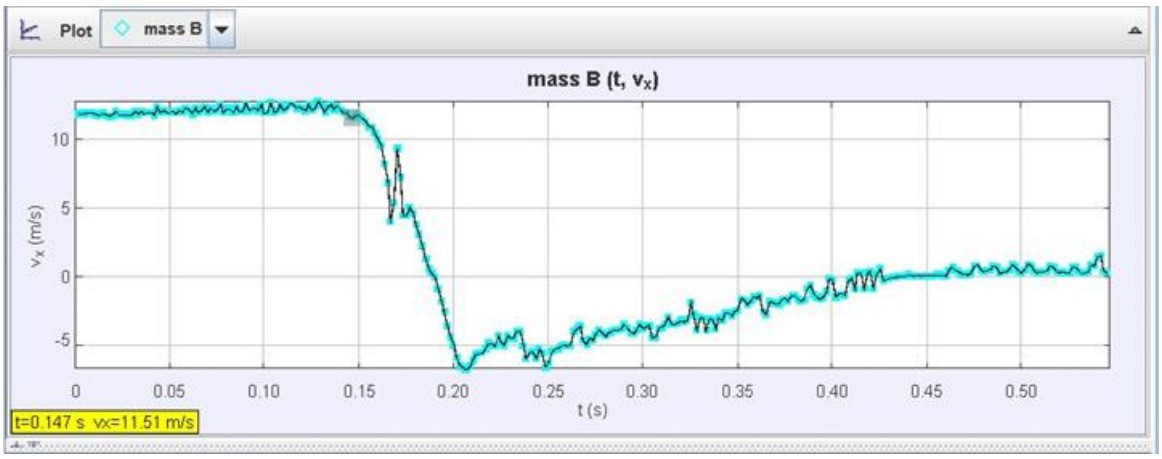

Figure 4.6 Velocity parameter graph

The data obtained for all parameters (x – displacement; v – velocity, a – acceleration) are displayed in Tracker in tabular form. The data regarding the velocity of the occupant's head will be filtered to improve clarity. The procedure will be presented in subsection 4.3.2.

4.3 Data Processing Procedures

In experimental research, the application of appropriate data processing procedures is essential to ensure the accuracy of the analyses. Measurement errors affect the recorded parameters, which may lead to data that do not reflect reality. To enhance data clarity and facilitate their interpretation, filtering methods are applied.

4.3.1 Measurement Errors

The parameters recorded for a road accident can be influenced by several factors that cause errors leading to data that does not reflect reality, such as: weather conditions, road conditions, vehicle characteristics, as well as incorrect data recording due to human factors [43].

Measurement errors are of two types: errors caused by incomplete acquisition of experimental data, as well as those generated by lack of precision in data collection [44].

Low accuracy can be caused by the precision of measuring instruments or by the way the measurement is performed; for example, if the radar device is positioned in different locations or at different distances from the vehicle for the two measurements (for example, placed at points such as the beginning and the end of the track). The time interval between the two measurements is also important.

Therefore, in order to quantify uncertainties, the bias or systematic error can be determined, based on the following analytical relationship:

$$b = B \pm \Delta b \tag{4.1}$$

Where:

b - calculated or measured value; B – reference value; Δb – variation of value b; b – B = bias or systematic error [45].

In the case of measured accelerations, bias correction, described in subchapter 4.2.2, is automatically implemented in the PocketDAQAnalyzer software application.

4.3.2 Data Filtering Methods

Origin is a data analysis and processing software widely used in scientific and engineering fields. In particular, it has proven effective for filtering raw data from crash tests. An experimentally obtained signal, through measurement, must be adjusted during its processing because filtering improves clarity. This is essential for identifying specific events or characteristics from crash test data, such as the exact moment of impact, peak velocity or acceleration values. Smoothed data plots are easier to read and interpret, which is essential for communicating results to stakeholders. Origin provides several methods that can be used to smooth raw experimental data [46]. For filtering data obtained in the field of accidentology, a filter using FFT can be applied.

For the experiment described in subchapter 4.2.3, the raw data regarding the occupant's head velocity were filtered. An FFT filter tuned to 15 window points was used.

To determine the velocity at the moment of impact, the data can be entered into Microsoft Excel. The occupant's head velocity was 12.36 m/s (Figure 4.7).

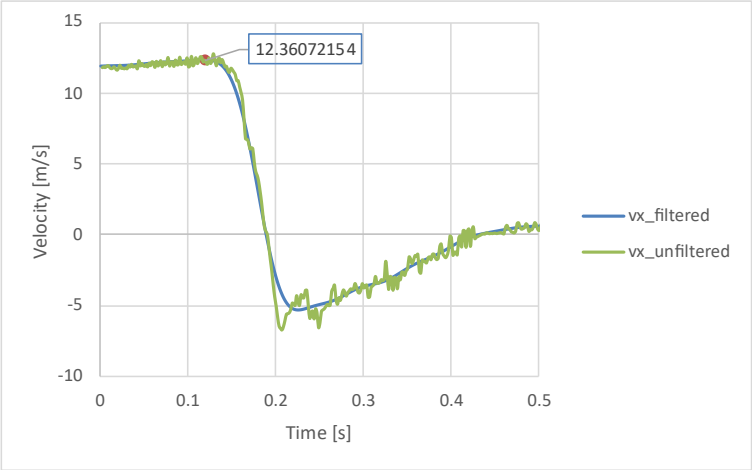

Figure 4.7 Graph with raw and smoothed data

4.4 Conclusions

This chapter presented the equipment and software applications used in experimental accidentology tests. Parameters such as vehicle speed can be acquired with the GPS system, while the accelerations of the vehicle and the occupant can be recorded with the PicDAQ systems. The kinematic parameters (displacement, velocity, acceleration) of the vehicle and occupants can be determined with the Tracker application using video recordings.

The presentation of the applications was carried out following experimental research and simulations. Various aspects of the software applications were highlighted, such as: the graphical interfaces of the applications used, as well as the working methodologies for their correct use. In addition, measurement errors and filtering methods after data acquisition were analyzed.

In conclusion, the use of the equipment and software applications presented contributes to road accident analysis, providing effective tools for the acquisition and interpretation of experimental data. The integration of the described methodologies facilitates not only the understanding of the phenomena that occur during impact but also the development of road safety solutions based on detailed analyses. By correctly applying the procedures and using filtering tools, measurement errors are reduced, and results are obtained that are as close to reality as possible.

5 METHODOLOGY OF EXPERIMENTAL RESEARCH

5.1 Establishing the Objectives of Experimental Testing

The experiments aim to evaluate the ability of a technical solution to reduce the risk and severity of occupant injuries in the event of a frontal collision between a vehicle and a rigid barrier. To this end, several stages were established, including the design and construction of the technical solution, impact simulations, measurements and analyses of vehicles and occupants behavior; followed by the calculation of injury criteria, based on which the severity and probability of injuries are determined. Subsequently, conclusions are drawn regarding the efficiency of the technical solution.

5.1.1 The Importance of Establishing Experimental Research Objectives

The objectives provide a framework for structuring the experiments. By defining clear goals, good planning of the experiments is ensured. This provides a basis for adaptive learning, where researchers can repeat experiments based on initial findings. This iterative process helps refine the objectives and improve methodologies.

5.1.2 Objectives of the Experiments

The main objective of experimental testing is to evaluate the capability of a technical solution that can effectively reduce the risk and severity of occupant injuries.

In order to achieve this objective, the following work program was developed:

1. Design and construction of a shock absorption system intended for occupant protection;

2. Simulation of the impact between a vehicle and a rigid barrier;

3. Simulation of the impact between a vehicle equipped with a shock absorption system and a rigid barrier;

4. Evaluation of the kinematic parameters (velocity, acceleration) corresponding to the vehicles and occupants involved in the collision;

5. Determination of the kinematic parameters obtained during the impact;

6. Calculation of the injury criteria at head and thorax level;

7. Determination of the severity of occupant injuries and the probability of injury occurrence;

8. Conclusions.

5.2 Establishing the Test Scenarios

Establishing the test scenarios is an essential step in evaluating the behavior of vehicles and occupants under frontal impact conditions. For this purpose, the necessary equipment was identified and a testing program was developed, structured into the preliminary procedure and the actual testing procedure. This included preparing the test track, the test vehicles, anthropomorphic devices, and the necessary equipment, thus ensuring optimal conditions for conducting the experiments. The proposed scenarios targeted frontal collisions between a vehicle and a rigid barrier, with and without the use of a shock absorption system.

5.2.1 Equipment and Testing Conditions

1. Test track: A specially arranged area for impact tests within the Research and Development Institute of Transilvania University of Brasov (Figure 5.1); Within the test track, a fixed, non-deformable concrete barrier was installed with the following dimensions: L = 185 cm; W = 185 cm; H = 115 cm.

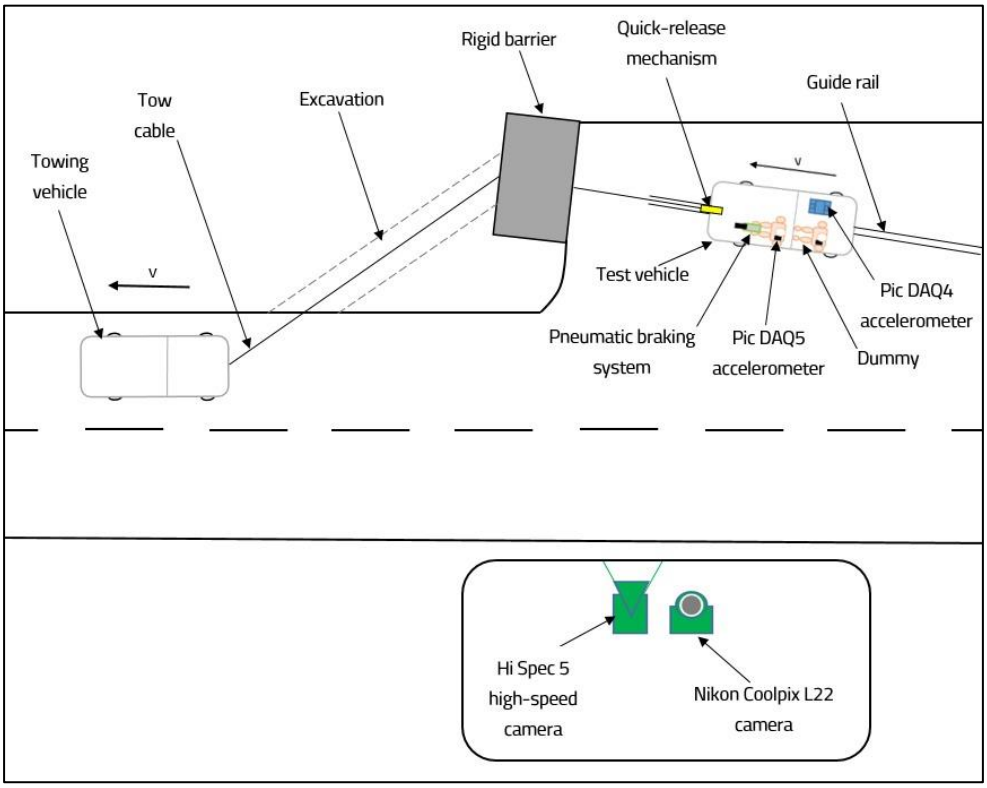

Figure 5.1 Test track

2. Quick-release mechanism: Device for releasing the test vehicle under load before impact;

3. Tow cable (85 m);

4. Guide rail: The rail is used to ensure a straight trajectory of the vehicle during towing;

5. Towing vehicle: The vehicle used for towing the test vehicle;

6. Two test vehicles (Figure 5.2);

Figure 5.2 Test vehicles

7. Data acquisition system (PicDAQ 4): Device for recording vehicle acceleration during impact;

8. Data acquisition system (PicDAQ 5): Device for recording dummy acceleration during impact;

9. Pneumatic braking system, electronically controlled, composed of:

-Compressed air tank (8 bar) and FESTO pneumatic cylinder for brake actuation;

-Electronic control module, pneumatic solenoid valves, connection hoses, and mounting support.

The pneumatic braking system is used as a protection system in case anomalies are detected and can stop the vehicle during the test run. Braking is triggered remotely from a maximum distance of 250 m.

10. Hi Spec 5 high-speed camera: The camera is used to record video footage during experimental tests. It has a memory capacity of 4 GB and is capable of recording at over 1400 frames per second. The device provides high-resolution images of 1696 x 1710 pixels [47];

11. Nikon Coolpix L22 camera: The digital photo-video camera was used on the test track for photographs taken during the preparation, execution, and after the experiments;

12. DJI Phantom 3 Standard drone: The drone was used to capture panoramic images. It weighs 1216 g, has a maximum take-off speed of 5 m/s, and a landing speed of 3 m/s. The drone can operate at temperatures between 0 and 40°C [48];

13. Two Anthropomorphic Test Devices – DD1 Prototype: The dummies were developed to study the kinematics of body movement in experimental tests. The device in Figure 5.3 has a total mass of 84.12 kg, distributed as follows: head 4.7 kg, neck 1.4 kg, upper torso 20 kg, lower torso 12.6 kg, the rest of the mass being distributed in the lower limbs.

Figure 5.3 Dummy (DD1 Prototype)

14. Shock absorption system: The system consists of a plastic support (Figure 5.4 a) with dimensions of 1231 mm width, 241 mm depth, 160 mm height, and 45 plastic containers filled with water (energy accumulators). The caps were perforated. The equipment was designed to reduce the effects of a vehicle collision with a rigid obstacle (Figure 5.4 b).

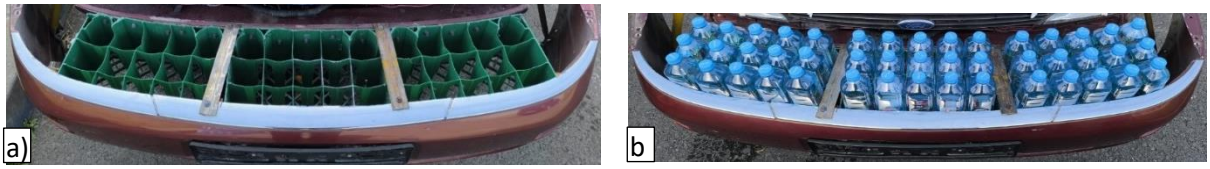

Figure 5.4 a) Plastic support of the shock absorption system ; b) Shock absorption system

5.2.2 Establishing the Testing Schedule

The program included preparation and execution phases to ensure that the tests would be carried out rigorously and safely.

Preliminary Procedures:

1. Inspection and calibration:

-Vehicles: Checking the technical condition of the vehicles;

-Dummies: Ensuring that the dummies meet the research purpose;

-Measuring Equipment: Calibrating and verifying the correct operation of the data acquisition devices.

2. Tests:

-Synchronization of equipment and operators: Ensuring the coordinated and safe operation of all equipment and proper involvement of researchers.

Testing Procedure:

a) Preparation of the test track;

b) Preparation of the test vehicle:

-Technical inspection: Full verification of the vehicle to confirm operational condition;

-Installation of measuring devices: Mounting the necessary equipment for data recording;

-Alignment on the towing rail: Positioning the vehicle on the guide rail to ensure a straight trajectory towards the fixed, undeformable barrier.

c) Preparation of anthropomorphic devices:

-Technical inspection: Full verification of the dummies to determine operational condition;

-Installation of data acquisition systems: Mounting the necessary equipment for data recording;

-Positioning of the dummies: Placing the dummies in the correct position to simulate real vehicle occupants.

d) Preparation of the equipment used for experiments;

e) Conducting the experimental tests.

5.2.3 Description of Test Scenarios

The first test scenario consisted of a frontal impact between a vehicle and a rigid barrier at a velocity of 42 km/h. The scenario is shown in Figure 5.5.

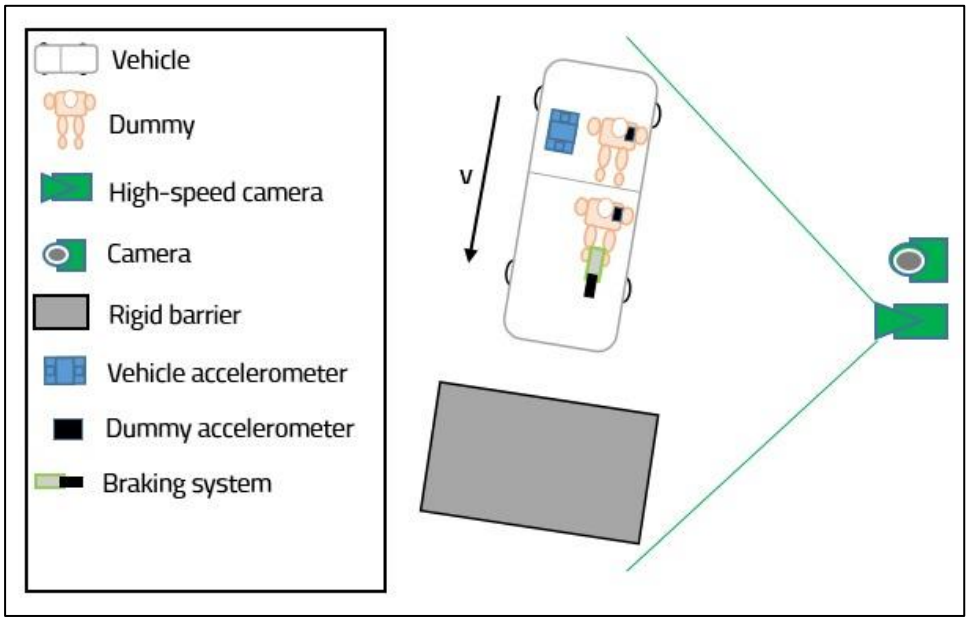

Figure 5.5 Collision scenario without shock absorption system

The second test scenario consisted of a frontal impact between a vehicle equipped with a shock absorption system and a rigid barrier at a velocity of 42 km/h. The scenario is shown in Figure 5.6.

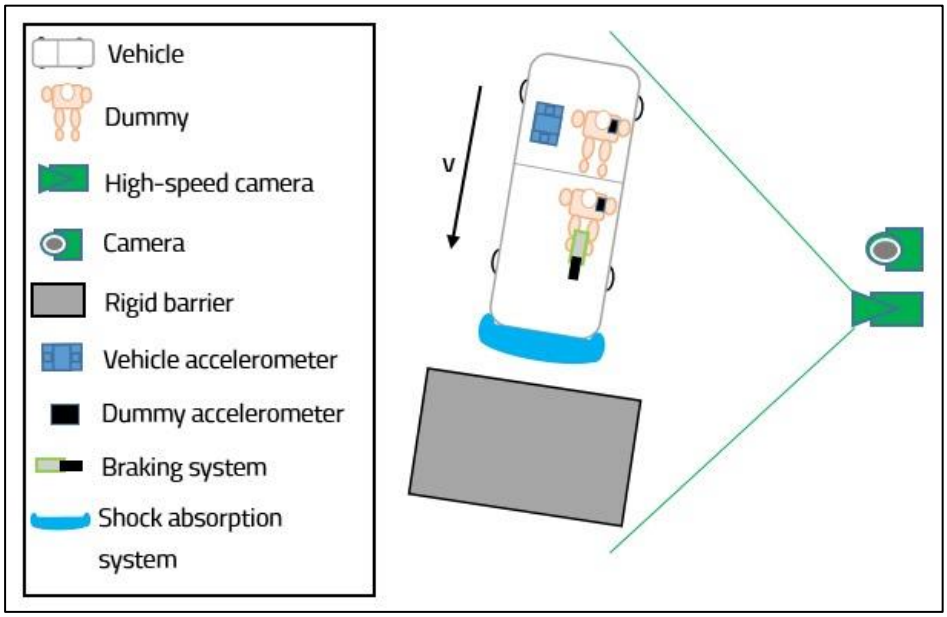

Figure 5.6 Collision scenario with shock absorption system

5.3 Preparation for Experimental Testing

The test track was arranged by delimiting the perimeter, preparing the towing system, as well as securing the rigid obstacle and the safe stopping space. Regarding the vehicles, preparation included checking the technical condition, installing the shock absorption system, applying the markings necessary for kinematic parameter analysis, and installing the data acquisition equipment. The test dummies were checked, equipped with sensors for monitoring kinematic parameters, and properly placed inside the vehicles. The data recording equipment was activated before starting the experiments.

5.3.1 Preparation of the Test Track

The experimental tests were carried out on the test track of the Research and Development Institute of Transilvania University of Brașov. For the preparation of the tests, the following steps were taken:

1. Delimitation of the test polygon

-Marking and delimiting the perimeter of the polygon.

2. Securing the stopping area

-Arranging a space intended for the safe stopping of the vehicles involved in the tests.

3. Preparation of the towing system

-Pretensioning the towing cable, with a length of 85 meters, necessary for setting in motion the vehicles used for the experimental tests.

4. Securing the barrier (concrete block) for tests.

5. Guiding the towing cable

-Creating an excavation to prevent friction between the ground and the towing cable, ensuring the safe operation of the system.

5.3.2 Preparation of the Vehicles

For the preparation of the two vehicles, the following steps were taken:

-Checking the braking systems and steering mechanisms;

-Installing the energy-absorbing system on the front part of the vehicle (Figure 5.7);

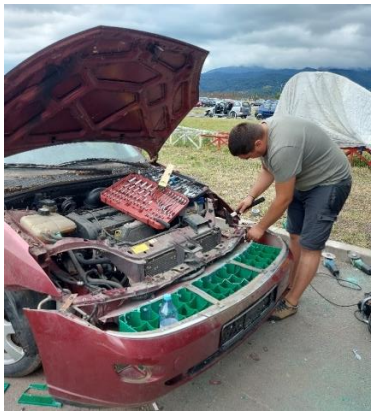

Figure 5.7 Installation of the energy-absorbing system

-Marking the tires according to the Euro NCAP model – The marking of the tires is necessary to monitor the rolling of the vehicles during the experiments and to detect any wheel locking;

-Applying markings on the car bodies (Figure 5.8) – The strips applied to the vehicle hoods are necessary for interpreting the deformations in the front part. They are applied at intervals of 200 mm, forming rectangular markings. On the sides of the vehicles, strips were applied at distances of 100 mm to establish reference length for video analysis. In addition, circular markings were applied on the bodywork to track mass points during video data processing.

Figure 5.8 Application of markings

-Checking the tire pressure;

-The PicDAQ 4 accelerometer was mounted on both vehicles (Figure 5.9). It was used for acquiring acceleration data during the experimental tests. The data acquisition system was mounted longitudinally on the rear floor of the vehicles;

Figure 5.9 Area for installing the PicDAQ 4 accelerometer

- The braking system was then installed;

- The cable guide rail was mounted perpendicular to the front side of the concrete barrier. Subsequently, the vehicles were placed, successively, on the guide rail in the initial test position.

5.3.3 Preparation of the Crash Test Dummies

Preparation of the dummies consisted of checking the neck and the joints at the limb level.

For acquiring the occupants' acceleration, the PicDAQ 5 data acquisition platform was used. The accelerometer was mounted inside the thorax (Figure 5.10).

Figure 5.10 Installation of the PicDAQ 5 accelerometer inside the dummy's thorax

After checking both dummies, they were positioned inside the vehicles (Figure 5.11). Both anthropomorphic test devices were equipped with seat belts.

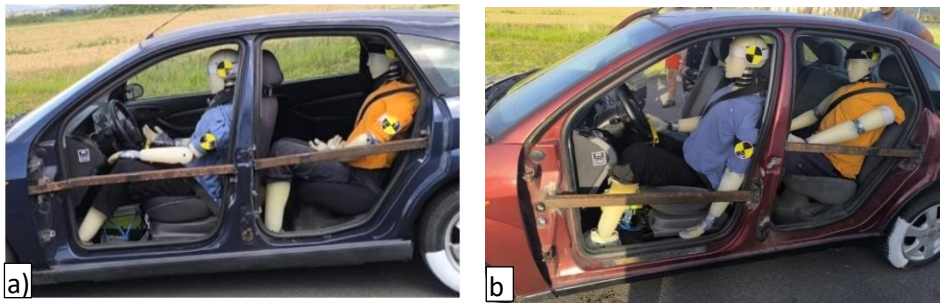

Figure 5.11 Positioning of the dummies in the vehicles: a) standard vehicle b) vehicle equipped with energy-absorbing system

5.3.4 Preparation of the Equipment

Before starting the tests, an evaluation was carried out on the battery charge level of the data acquisition platforms, the photo and video cameras, as well as the drone. The last step in preparing the equipment was the activation of the data acquisition platforms (PicDAQ 4 corresponding to the vehicle and PicDAQ 5 corresponding to the anthropomorphic test device).

5.4 Conducting the Experimental Tests

A preliminary test was carried out to observe whether the vehicles follow a precise, straight trajectory toward the rigid barrier. Subsequently, the two vehicles were connected to a towing system and propelled forward. At the end of the verification, the braking system was activated to stop the vehicles before reaching the rigid barrier.

5.4.1 Conducting the Vehicle - Rigid Barrier Impact Test

Experimental test coordinates: date / time: June 26, 2024 / 17:00; in the towed vehicle, with two dummies installed — one in the driver's seat and one in the rear passenger seat; the dummies were secured with

three-point seat belts, and the vehicle was equipped with a steering-wheel airbag; frontal impact; velocity at the moment of collision with the barrier: 42 km/h. The vehicle was launched using the towing system. The kinematics of the impact is shown in Figures 5.12-5.14.

Figure 5.12 Impact kinematics at t=0 s

Figure 5.13 Impact kinematics at t=0.1 s

Figure 5.14 Impact kinematics at t=0.2 s

5.4.2 Conducting the Experimental Test of a Vehicle Equipped with an Energy-Absorbing Device - Rigid Barrier

Experimental test coordinates: date / time: June 20, 2024 / 19:00; in the towed vehicle, with two dummies installed — one in the driver's seat and one in the rear passenger seat; the dummies were secured with three-point seat belts, and the vehicle was equipped with a steering-wheel airbag; frontal impact; velocity at the moment of collision with the barrier: 42 km/h. The vehicle was launched using the towing system. The kinematics of the impact is shown in Figures 5.15-5.17.

Figure 5.15 Impact kinematics (t=0 s)

Figure 5.16 Impact kinematics (t=0.1 s)

Figure 5.17 Impact kinematics (t=0.2 s)

After the vehicles came to a complete stop, the data acquisition equipment was deactivated.

5.5 Conclusions

This chapter detailed the experimental research methodology applied to the preparation and execution of collision tests.

Proper implementation of a testing program can be ensured through real frontal impact scenarios. Careful verification and calibration of equipment, meticulous preparation of the vehicles, and correct positioning of the dummies are essential for conducting experiments with a high level of confidence. The results of these tests contribute to the development of technical solutions for protection systems, having a direct impact on increasing road safety for traffic participants.

The presented accidentology experiment provides a detailed and accurate understanding of the behavior of vehicles and occupants during a collision. The rigorous preparation procedures, including verification of the straight trajectory of the tested vehicle and the use of the braking system in the preliminary test, ensured controlled and reproducible testing conditions.

Within the experimental research methodology, the procedures were essential for eliminating uncontrolled variables and reducing the risk of errors. Creating controlled and reproducible testing conditions is the foundation on which subsequent analyses will be based. The preliminary measurements ensured that the experiment could proceed as planned, allowing the collection of useful data for a detailed understanding of the studied phenomena.

6 DATA PROCESSING AND ANALYSIS

6.1 Determination of Impact Parameters

Depending on the test configuration, the data regarding the vehicle velocity, as well as the head and thorax of the occupant, were determined by processing the video samples using the Tracker software application. The accelerations were recorded with the PicDAQ 4 and PicDAQ 5 data acquisition platforms. The measurements were later compared to evaluate the influence of the energy-absorbing system.

6.1.1 Determination of the Kinematic Parameters of the Vehicle and Occupants from the Experimental Test Vehicle - Rigid Barrier

The velocities of the vehicle, as well as the head and thorax of the occupant, were determined using the Tracker software application. This consisted of loading the video sample recorded with the high-speed camera. The calculated velocity parameter was processed using the Origin application. The velocity values corresponding to the X-axis are important; therefore, the vehicle velocity along the Y-axis was neglected. The raw data were filtered using an FFT filter, with the smoothing level set to 35 window points. As with the vehicle, it was considered that the relevant velocity for analyzing the kinematics of the occupants is along the X-axis, as this corresponds to the direction of motion and provides an accurate representation of the dummy's displacement relative to the collision trajectory.

The acceleration of the vehicle was acquired using the PicDAQ4 accelerometer. The collected data were filtered with a CFC 60 filter, according to SAE J211/1 standard. The accelerations of the driver and passenger were recorded using the PicDAQ5 equipment and filtered with a CFC 1000 filter for head accelerations and CFC 180 for thorax accelerations, according to SAE J211/1 standard. The data were later processed in Microsoft Excel.

6.1.2 Determination of the Kinematic Parameters of the Vehicle and Occupants from the Experimental Test Vehicle with Impact Attenuation System - Rigid Barrier

Similar to the procedure described in subchapter 6.1.1, the velocities and accelerations of the vehicle and occupants were determined.

6.1.3 Comparative Analysis of Kinematic Parameters

Following the execution of the two impact tests, the values of the velocities and accelerations acting on the vehicles, as well as on the head and thorax of the occupants, were compared. The emphasis was placed on comparing the minimum and maximum accelerations resulting from the impact and on evaluating the level of protection offered by the vehicle and by the energy-absorbing system mounted on one of the vehicles.

To allow a detailed evaluation, the velocity and acceleration parameters for each of the two tests were organized in a comparative table (Table 6.1).

Table 6.1 Kinematic parameter values obtained from the tests

		Test 1 (Vehicle - rigid barrier)	Test 2 (Vehicle with shock absorption system - rigid barrier)
Vehicle	Impact velocity [m/s]	11.67	11.74

	ax [m/s^2]	Min	-283.31	-259.21
		Max	7.36	41.51
	ay [m/s^2]	Min	-17.09	-69.27
		Max	22.32	26.26
	az [m/s^2]	Min	-124.65	-149.05
		Max	103.11	131.28
Driver's head	Impact velocity [m/s]		11.28	11.45
	ax [m/s^2]	Min	-278.62	-267.86
		Max	0.92	10.91
	ay [m/s^2]	Min	-48.29	-47.41
		Max	45.48	48.69
	az [m/s^2]	Min	-306.32	-264.63
		Max	7.56	10.70
Driver's thorax	Impact velocity [m/s]		11.44	11.46
	ax [m/s^2]	Min	-316.39	-294.696
		Max	37.76	10.68
	ay [m/s^2]	Min	-164.92	-96.87
		Max	24.26	27.68
	az [m/s^2]	Min	-127.10	-77.15
		Max	21.90	27.13
Passenger's head	Impact velocity [m/s]		11.04	10.85
	ax [m/s^2]	Min	-475.32	-340.31
		Max	9.42	7.52
	ay [m/s^2]	Min	-68.46	-77.44
		Max	23.91	11.73
	az [m/s^2]	Min	-242.09	-174.36
		Max	4.22	5.40
Passenger's thorax	Impact velocity [m/s]		11.33	11.26
	ax [m/s^2]	Min	-408.76	-301.66
		Max	93.995	1.89
	ay [m/s^2]	Min	-176.02	-141.03

		Max	50.81	42.89
	az [m/s^2]	Min	-59.93	-46.82
		Max	83.56	45.85

To visually illustrate the differences between the two tests, graphs were created for each entity (vehicle, head, thorax) separately. Each graph shows the variation of velocities and accelerations recorded during the impact.

It can be observed that in the case of the vehicle equipped with an energy-absorbing device activated at the moment of impact, the velocity evolution along the X-axis is slower compared to that of the vehicle without the energy-absorbing system (Figure 6.1). It is found that the time after which the velocity is reduced to zero is Δt=0.013 seconds longer in case 2, which leads to the conclusion that the vehicle acceleration is reduced.

The comparative acceleration graph of the two vehicles along the X-axis shows that the maximum deceleration of the vehicle occurs with a delay of approx. 0.013 s in case 2, and the dynamic loads are lower. In the case of acceleration and deceleration along the Y and Z axes, the measurements indicate an increase for the vehicle equipped with the energy-absorbing system. This phenomenon is due to the redistribution of vertical forces caused by the expulsion of water from the containers that make up the shock absorption system.

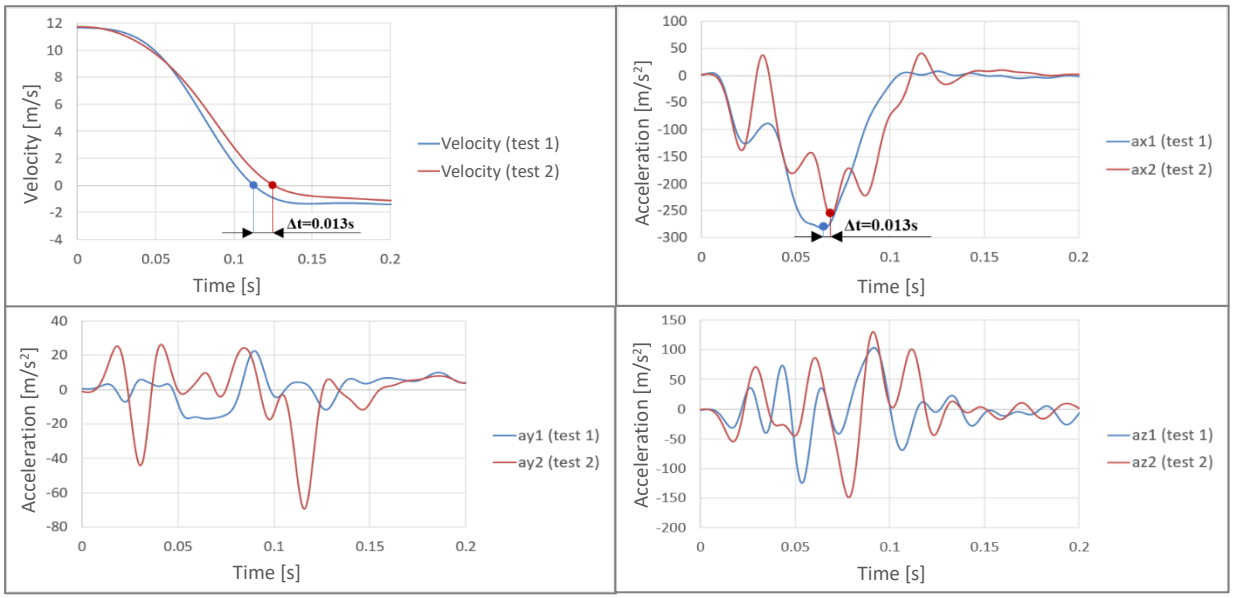

Figure 6.1 Velocities and accelerations of the two vehicles

The graph of velocity variation on the X-axis (Figure 6.2), at the level of the dummy's head positioned on the driver's seat, indicates that although the velocity before the impact is similar in both test configurations, as in the case of the vehicle, in test 2 there is a delay (Δt=0.021s) when the velocity reaches 0 m/s.

The analysis of the acceleration recorded at the level of the dummy's head positioned on the driver's seat highlights differences between the two bumper design configurations. In test 2, with a delay of approx. 0.021 s, the maximum deceleration is reduced along the X-axis. For the Y-axis acceleration of the dummy's head, it can be seen that its minimum value is reduced. The comparative acceleration graph at head level, on the Z-axis, indicates that the occupant of the vehicle equipped with the energy-absorbing device experienced lower minimum accelerations compared to those experienced by the occupant of the vehicle without the shock absorption system.

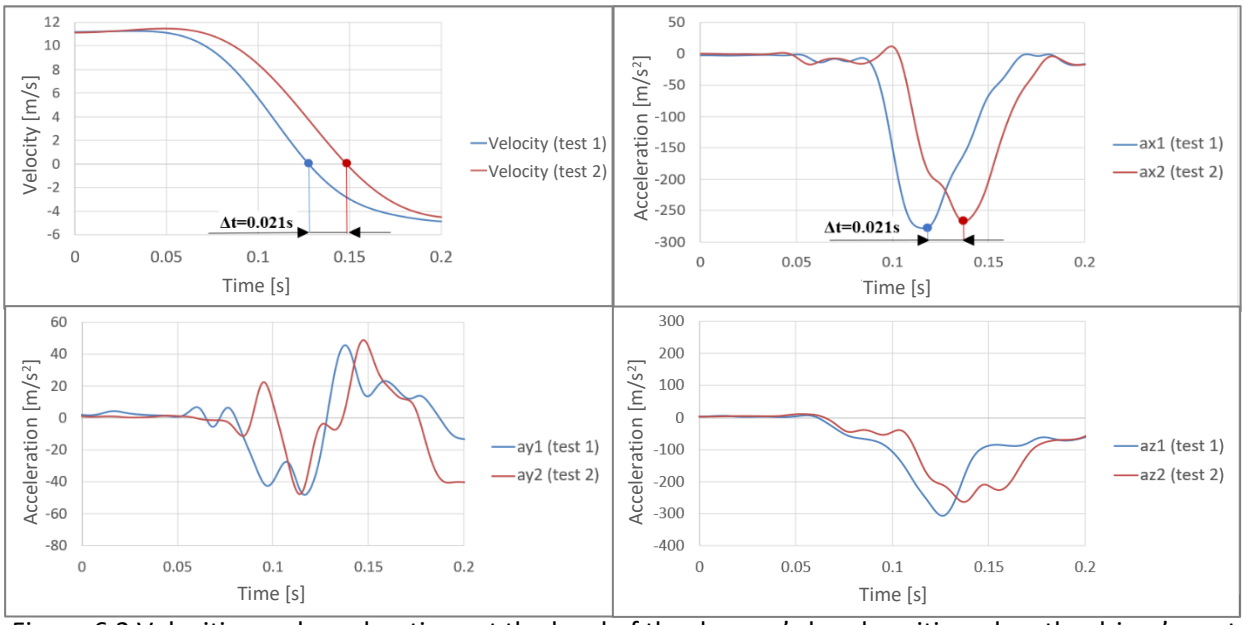

Figure 6.2 Velocities and accelerations at the level of the dummy's head positioned on the driver's seat

The analysis of velocity recorded on the X-axis, at the level of the dummy's thorax positioned on the driver's seat shows that, in both configurations, the thorax velocity before the collision is identical, but in the case of the vehicle with the energy-absorbing system, the velocity reaches zero after 0.018 s (Figure 6.3).

The comparative graphs of the acceleration at the dummy's thorax level on the X, Y, Z axes show a clear reduction of the minimum acceleration endured by the occupant on all three axes when the vehicle was equipped with an additional impact shock attenuation system, indicating efficient mitigation of the impact energy. In test 2, the maximum deceleration on the X-axis was obtained with a delay of approx. 0.018 s.

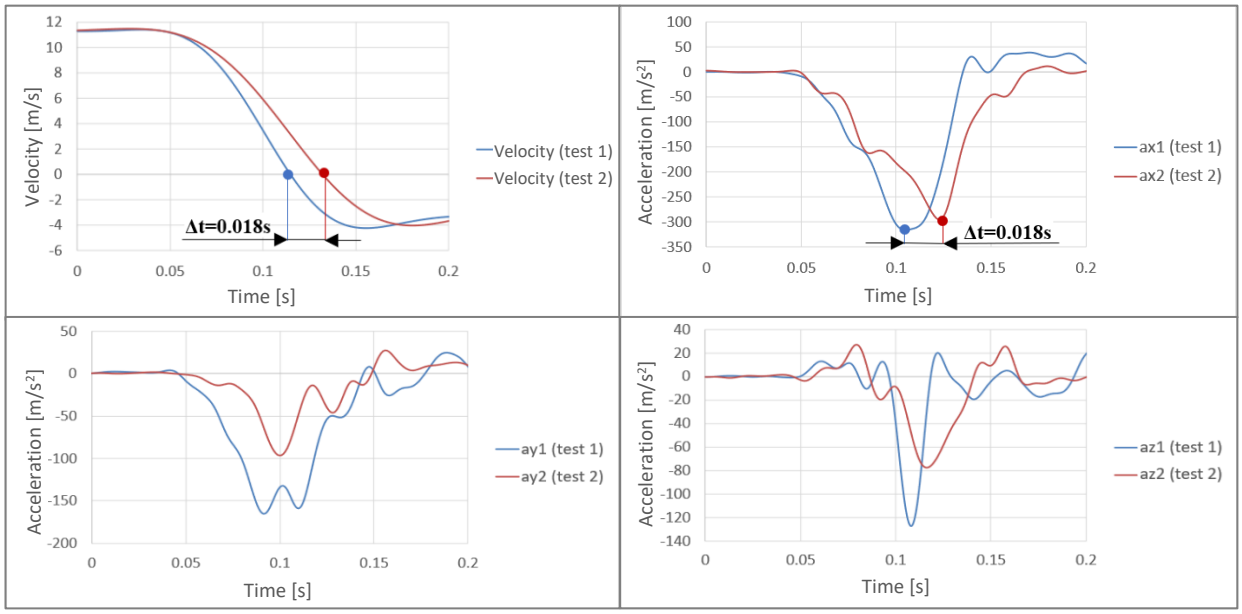

Figure 6.3 Comparative graphs of velocity and acceleration at the level of the dummy's thorax positioned on the driver's seat

The analysis of velocity on the X-axis, recorded at the level of the dummy's head seated in the rear passenger seat shows that before impact, it is comparable for both vehicle configurations (Figure 6.4). However, in the case of the vehicle equipped with the energy-absorbing device, the velocity reaches zero with a delay of Δt=0.022s.

The comparative graphs of head acceleration on the X, Y, and Z axes indicate a reduction of the maximum value on the Y-axis for the passenger in vehicle 2, and a decrease of the minimum acceleration on the Z and X axes (in this case, the delay was approx. 0.022s).

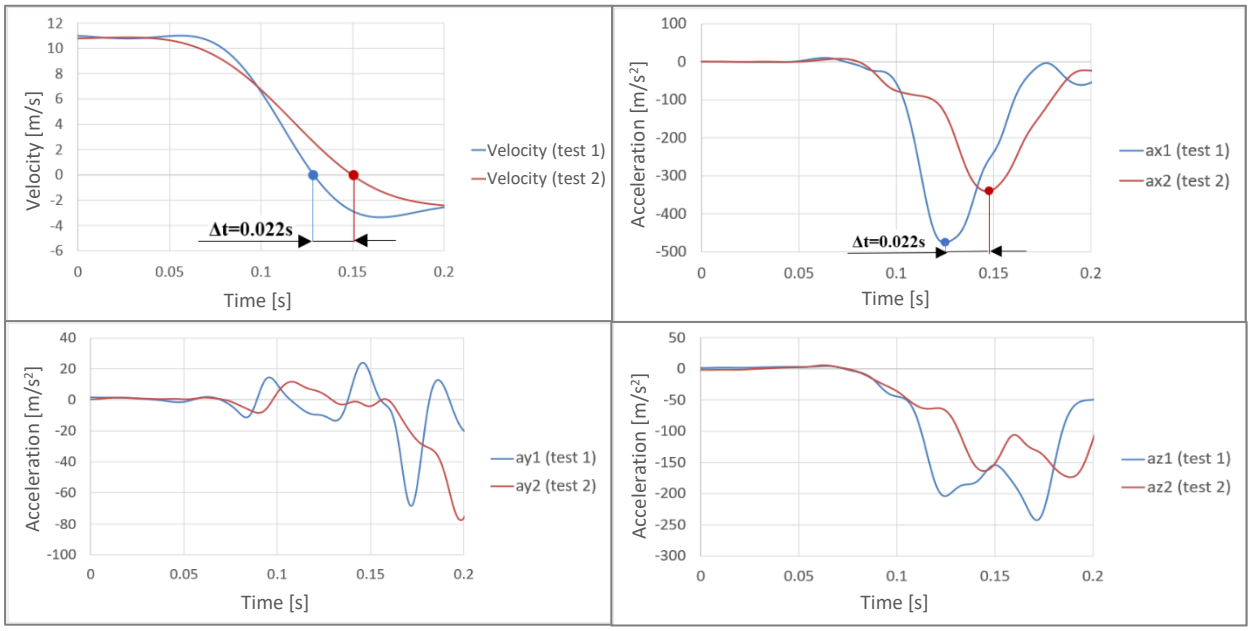

Figure 6.4 Comparative graphs of velocity and acceleration at the level of the dummy's head positioned on the rear passenger's seat

In the graph from Figure 6.5, the analysis of the dummy's thorax velocity positioned on the rear passenger seat shows that along the X direction, when it reached the value of 0 m/s, there was a delay of 0.019 s in test 2, indicating a reduction in deceleration.

The comparison of the acceleration recorded at the passenger's thorax level shows that both the minimum and maximum accelerations were reduced on all axes for the passenger in the vehicle equipped with the energy-absorbing system. For test 2, on the X-axis, the time at which the minimum acceleration is obtained increases by approx. 0.019 s.

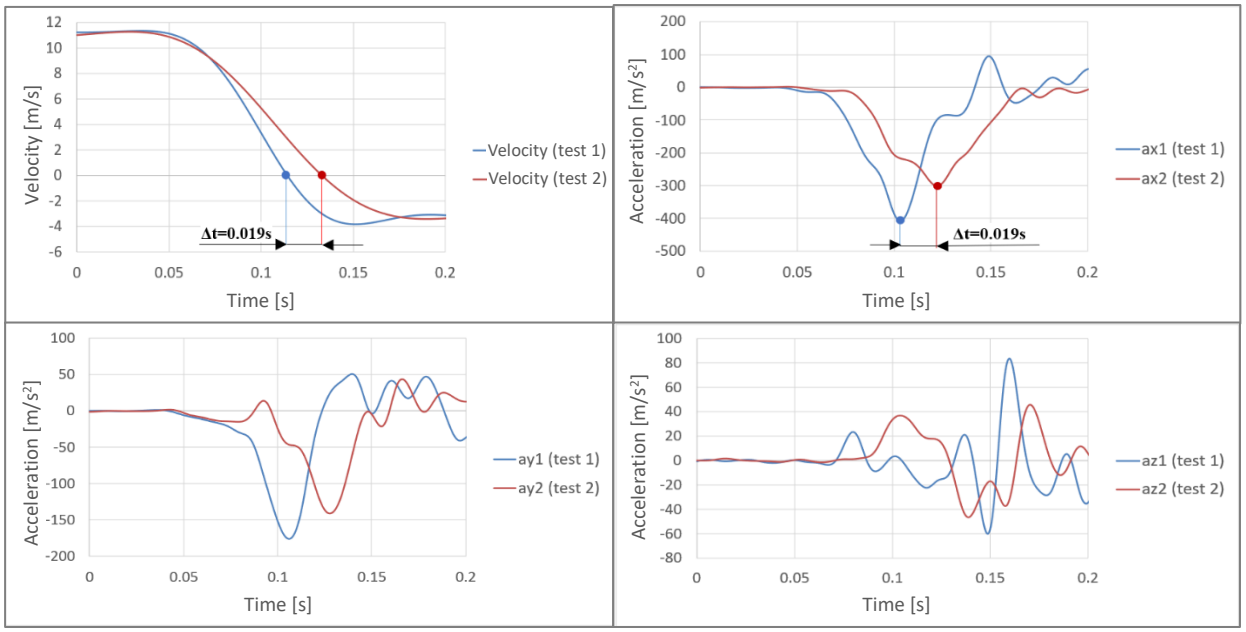

Figure 6.5 Velocity and acceleration at the level of the dummy's thorax positioned on the rear passenger's seat

6.2 Calculation of Injury Criteria

In Figure 6.6 (a), the variations of the acceleration measured at the driver's head are illustrated for the two experimental tests (max 40.03 g ≈ 392.7 m/s² for test 1 and 38.34 g ≈ 376.1 m/s² for test 2), which do not exceed the limit of 80 g (784.8 m/s²) over a duration of 3 ms according to UNECE R94. The 36 ms interval is marked on the diagrams. In Figure 6.6 (b), the evolution of HIC 36 over time is shown for the dummy positioned on the driver's seat. The maximum values obtained (256.66 for test 1 and 232.78 for test 2) meet both the UNECE R80 requirements (HIC < 500) and the upper limits imposed by UNECE R94 and FMVSS 208 (HIC ≤ 1000).

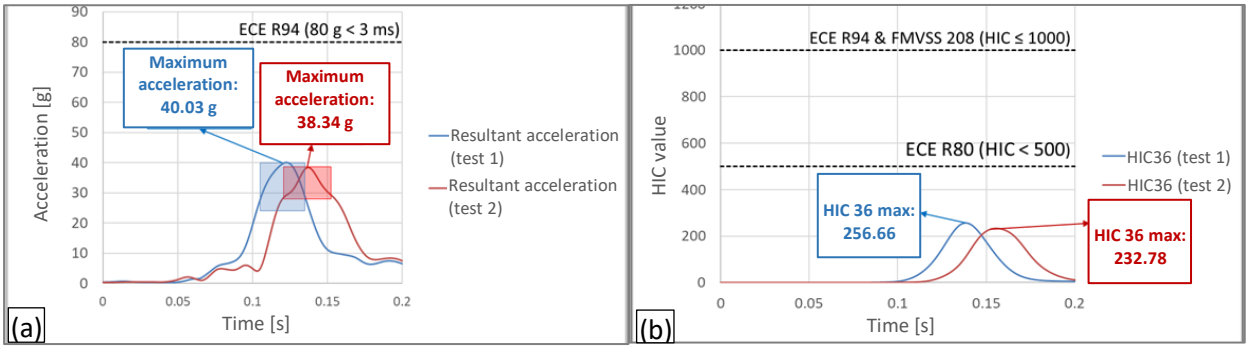

Figure 6.6 (a) Resultant acceleration at the driver's head with marking of the 36 ms interval for which the maximum HIC is determined; (b) Evolution of HIC 36 over time for the driver

In Figure 6.7 (a), the resultant accelerations at the dummy's (passenger's) head are presented, including the maximum values of 52.72 g (517.2 m/s²) for test 1 and 38.45 g (377.2 m/s²) for test 2. These are below the limit of 80 g (784.8 m/s²) specified by UNECE R94. The 36 ms time interval relevant for HIC calculation is highlighted in the same graph. In the case of the passenger, the graph of HIC 36 evolution, shown in Figure 6.7 (b), highlights the maximum HIC values (493.39 for test 1 and 229.14 for test 2). Compliance with biomechanical limits is confirmed since the calculated values are below 500 according to UNECE R80 and do not exceed 1000, in accordance with UNECE R94 and FMVSS 208.

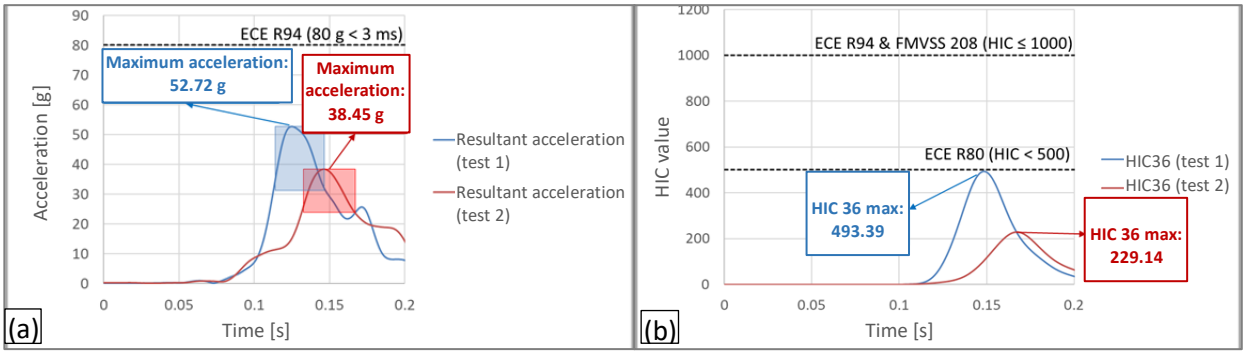

Figure 6.7 (a) Resultant acceleration at the dummy's (passenger's) head with marking of the 36 ms interval for which the maximum HIC is determined; (b) Evolution of HIC 36 over time for the passenger

For the driver, the values obtained in both experimental tests are correlated with an index between 0 and 1 on the AIS scale, which is associated with no risk or low severity of injuries. For the passenger, positioned on the rear bench, in the first test the HIC value can be correlated with an index between 1 and 2, representing low to moderate injury severity, while in the second test the mitigation of injuries due to the energy-absorbing system is significant; the HIC value is correlated with an index between 0 and 1 on the AIS scale.

In Figure 6.8 (a), the variations of acceleration over time at the dummy's thorax positioned on the driver's seat are presented. The graph marks the ThAC max values (38.02 g ≈ 373 m/s² for test 1 and 30.92 g ≈ 303.3 m/s² for test 2), corresponding to the maximum thorax acceleration, as well as the critical intervals

in which the resultant acceleration exceeds the limit of 30 g (294.3 m/s²). The exceedance duration is 24 ms for test 1 and 6 ms for test 2. The calculated ThAC values do not satisfy UNECE R80 requirements, which limit the duration of exceedance above 30 g (294.3 m/s²) to 3 ms. However, they are within the limits imposed by FMVSS 208, where an acceleration of up to 60 g (588.6 m/s²) is allowed for a maximum duration of 3 ms. In Figure 6.8 (b), as in the case of the driver, the acceleration recorded at the passenger's thorax is plotted over time. The ThAC max values (45.14 g ≈ 442.8 m/s² for test 1 and 33.33 g ≈ 327 m/s² for test 2) are marked, corresponding to the maximum thorax acceleration, as well as the time intervals in which the acceleration exceeds the 30 g (294.3 m/s²) threshold. In this case, the exceedance duration is 19 ms for test 1 and 11 ms for test 2.

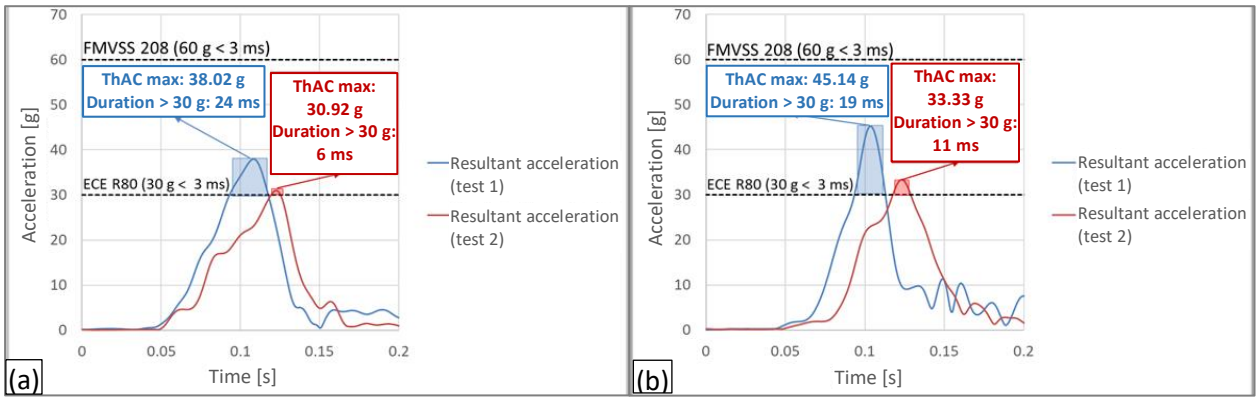

Figure 6.8 Resultant acceleration at the driver's thorax (a), and passenger's thorax (b), highlighting the ThAC value

The results obtained for both tests show that accelerations higher than 30 g (294.3 m/s²) exceed the maximum duration allowed of 3 ms specified in UNECE R80, but they meet the requirements of FMVSS 208, which allow accelerations up to 60 g (588.6 m/s²) for durations under 3 ms.

6.3 Comparative Analysis and Validation of the Mathematical Model

For the validation of the mathematical model developed in subchapter 3.1, the results obtained from the experimental tests are compared with those generated by simulation. The input parameters are determined based on the experimental data. Thus, the model's ability to reproduce the analyzed phenomenon is evaluated.

6.3.1 Input Parameters for Simulations

Validation of the mathematical model involves introducing several parameters determined from the experimental test data. For this purpose, an analysis of the deformations in the frontal area of the two tested vehicles was carried out. Scaled photographs were used. The amplitude of the deformed zone was 918.2 mm for both vehicles. For the vehicle in test 1, a detailed analysis of the distribution of deformations on the various surfaces of the grid ensured the determination of the average deformation of the affected area (324.5125 mm). For the vehicle equipped with the energy-absorbing system (test 2), the deformation was determined to be 478.4125 mm = 237.4125 mm + 241 mm. This includes both the structural deformation of the front part (237.4125 mm) and that of the energy-absorbing system with a thickness of 241 mm. Compared to the vehicle without the energy-absorbing system, the front part of the vehicle suffered less deformation. This suggests a more efficient dissipation of impact energy through the shock absorption system. It contributes to reducing direct structural deformation by extending the overall deformation zone.

For the calculations, the necessary input parameters were determined. Thus, an initial velocity of 42 km/h (≅11.7 m/s) was considered for both scenarios analyzed, with and without the energy-absorbing system. The determined mass of the vehicle without the energy-absorbing system was 1204 kg, while that of the

vehicle with the shock absorption system was 1255 kg = 1205 kg (vehicle curb mass) + 50 kg (shock absorption system mass). For the occupant, the same values as in the experiment were used: the mass of the thorax was 32.6 kg, and that of the head was 4.7 kg. In addition, the mass of the neck, estimated at 1.4 kg, was distributed proportionally, with 0.7 kg added to both the thorax and the head, to accurately reflect the mass distribution. This approach ensures consistency between the parameters used in the simulation and those specific to the experimental test. For the two analyzed vehicles, the input force to the system "F" was calculated based on the acceleration recorded during the impact on the X-axis and the sum of the vehicle mass and the occupant's mass:

Vehicle (test 1): $F = (1204\ kg\ + 84.12\ kg) \cdot 283.31\ m/s^2\ \cong 364{,}937.3\ N$

Vehicle (test 2): $F = (1255\ kg\ + 84.12\ kg) \cdot 259.21\ m/s^2\ \cong 347{,}113.3\ N$

The maximum deceleration used in the mathematical model, determined from the experimentally measured value, corresponds to the scenario in which the vehicle had two occupants. However, in the mathematical model, a single occupant was considered, given the need for simplification for system analysis. This approach allows correlation between the experimental conditions and the numerically simulated ones. The structural stiffnesses of the front part, for the two vehicles, were calculated by relating the force resulting from the product of the vehicle mass and the deceleration to the magnitude of the previously obtained deformation:

Vehicle (test 1): $k_1 = \frac{(1204\ kg \cdot 283.31\ m/s^2)}{0.3245125\ \mathrm{m}}\ \cong 1051131.3\ N/m$

Vehicle (test 2): $k_1 = \frac{(1255\ kg \cdot 259.21\ m/s^2)}{0.4784125\ \mathrm{m}}\ \cong 679975\ N/m$

The stiffness values corresponding to the restraint system (k_2) and the head (k_3) were taken from specialized publications as presented in subchapter 3.1.

6.3.2 Validation of the Mathematical Model

Validation of the mathematical model begins with determining the optimal fraction of the critical damping (ζ), which is a parameter for calibrating and analyzing the dynamic behavior of the system. In the case of test 1, the fraction of critical damping was determined through numerical simulations performed in Simulink, using damping coefficients calculated for fraction values between 0.1 and 0.7. The results indicate different optimal values for the vehicle (0.2), driver (0.4), and passenger (0.2). The optimal fractions were selected based on the minimum percentage errors calculated through MAPE: 2.3% for the vehicle, 15.3% for the driver, and 9.5% for the passenger. For the vehicle with the damping system (test 2), the results indicate the same optimal fraction (0.3) for both the driver and the passenger, associated with a minimum percentage error of 17.2% for the driver and 10.1% for the passenger. For the vehicle, the optimal fraction is different, being 0.1, with a minimum percentage error of 9.6%. To ensure a coherent comparison between test 1 and test 2, a calibration strategy using intermediate fractions was adopted. This methodology provides a balanced representation of the system's dynamics, avoiding discrepancies that may arise from using different fractions between tests. The recalibrated values are 0.15 for the vehicle, 0.35 for the driver, and 0.25 for the passenger. The damping coefficients corresponding to these fractions were calculated as follows:

Test 1: Vehicle ($\zeta = 0.15$): $c_1 = \zeta \cdot 2\sqrt{m_1 \cdot k_1}\ \cong 10672.4\ \frac{N*s}{m}$

Test 2: Vehicle ($\zeta = 0.15$): $c_1 = \zeta \cdot 2\sqrt{m_1 \cdot k_1}\ \cong 8763.7\ \frac{N*s}{m}$

Test 1 and test 2:

Driver's thorax ($\zeta = 0.35$): $c_2 = \zeta \cdot 2\sqrt{m_2 \cdot k_2}\ \cong 1629.8\ \frac{N*s}{m}$

Driver's head ($\zeta = 0.35$): $c_3 = \zeta \cdot 2\sqrt{m_3 \cdot k_3} \cong 322.3 \frac{N*s}{m}$

Passenger's thorax ($\zeta = 0.25$): $c_2 = \zeta \cdot 2\sqrt{m_2 \cdot k_2} \cong 1164.2 \frac{N*s}{m}$

Passenger's head ($\zeta = 0.25$): $c_3 = \zeta \cdot 2\sqrt{m_3 \cdot k_3} \cong 230.2 \frac{N*s}{m}$

An additional calibration step was necessary, consisting of adjusting the time shifts between the simulated and experimental responses. Thus, the model was adjusted to more accurately reproduce the temporal sequence of dynamic events for the occupants, while maintaining consistency with the real data. In contrast, the vehicle's response was confirmed to be representative from the initial stage, without requiring additional interventions. The time shifts calculated for the occupants showed faster responses in the simulation compared to those determined experimentally. For the driver, the thorax presented delays of 0.0423 s in test 1 and 0.0483 s in test 2, while the head had delays of 0.0473 s in test 1 and 0.0623 s in test 2. For the passenger, the delays were 0.0343 s for the thorax and 0.0503 s for the head in test 1, and 0.0413 s for the thorax and 0.0663 s for the head in test 2.

The mathematical model was solved over a duration of 0.2 s using the ODE45 algorithm.

For test 1, figures 6.9–6.13 present comparative responses of the vehicle, driver (head and thorax), and passenger (head and thorax), evaluated by velocity and acceleration obtained from experiment and simulation.

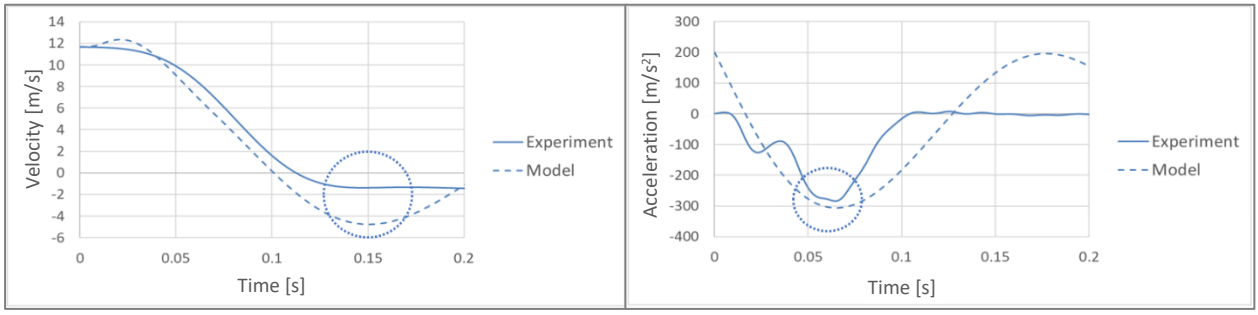

Figure 6.9 Comparison of vehicle velocity and acceleration: experiment and simulation for test 1

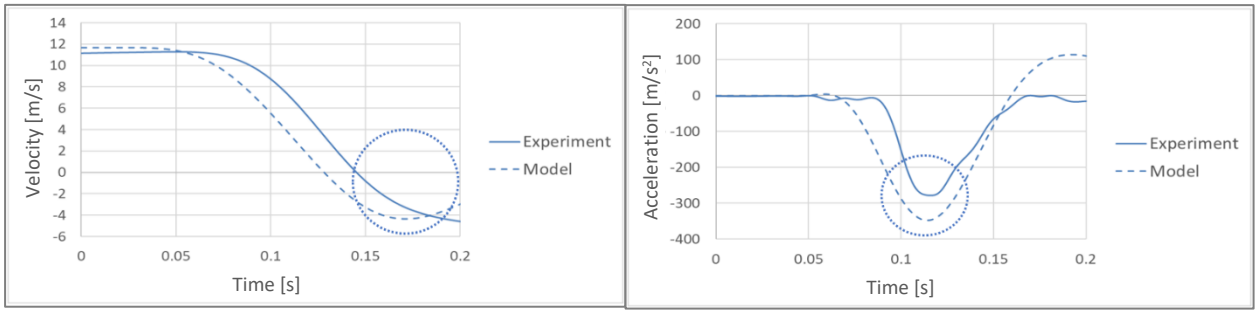

Figure 6.10 Comparison of driver's head velocity/acceleration: experiment and simulation (test 1)

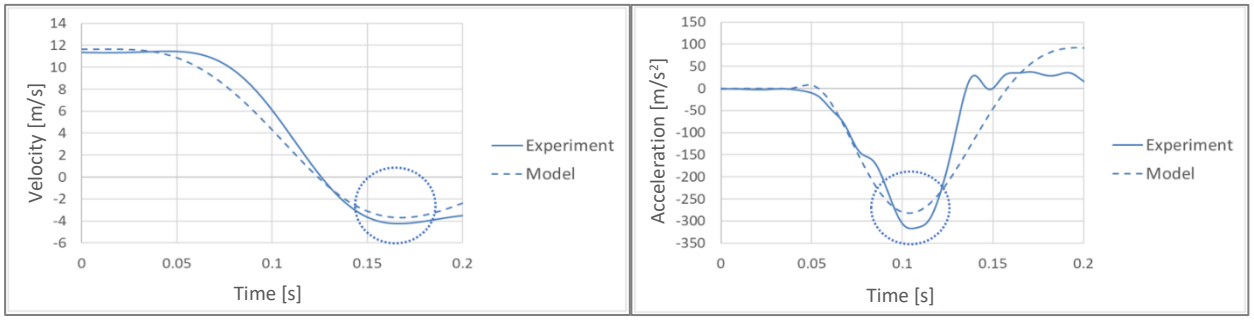

Figure 6.11 Comparison of driver's thorax velocity/acceleration: experiment and simulation (test 1)

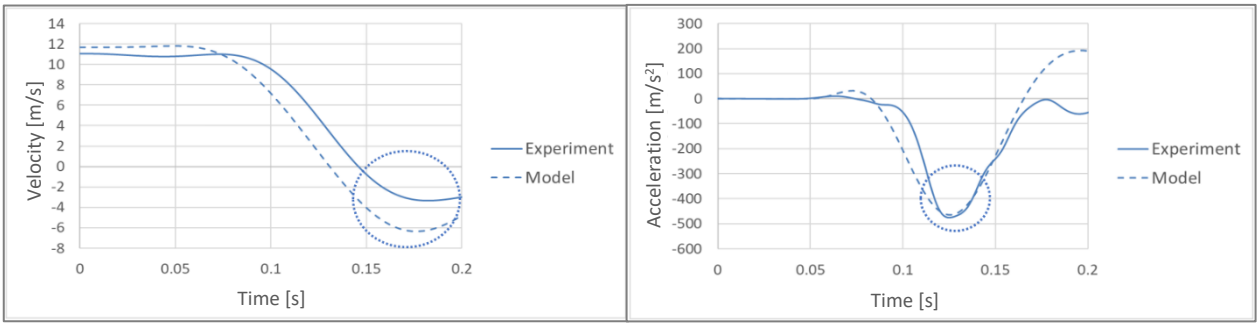

Figure 6.12 Comparison of passenger's head velocity/acceleration: experiment and simulation (test 1)

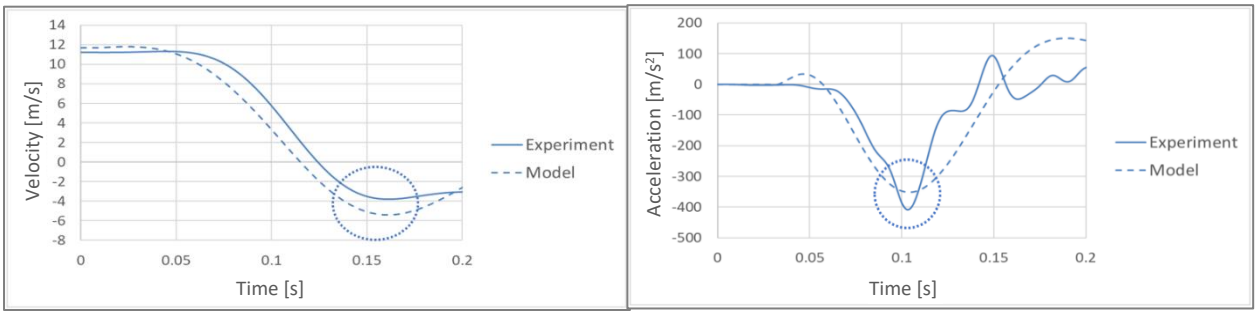

Figure 6.13 Comparison of passenger's thorax velocity/acceleration: experiment and simulation (test 1)

For test 2, figures 6.14–6.18 similarly illustrate the vehicle, driver's, and passenger's velocities and accelerations obtained from experiment and simulation.

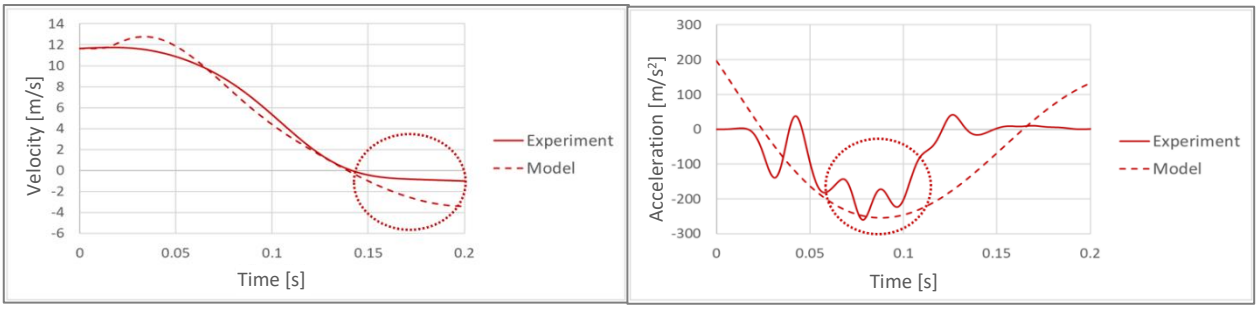

Figure 6.14 Comparison of vehicle velocity and acceleration: experiment and simulation for test 2

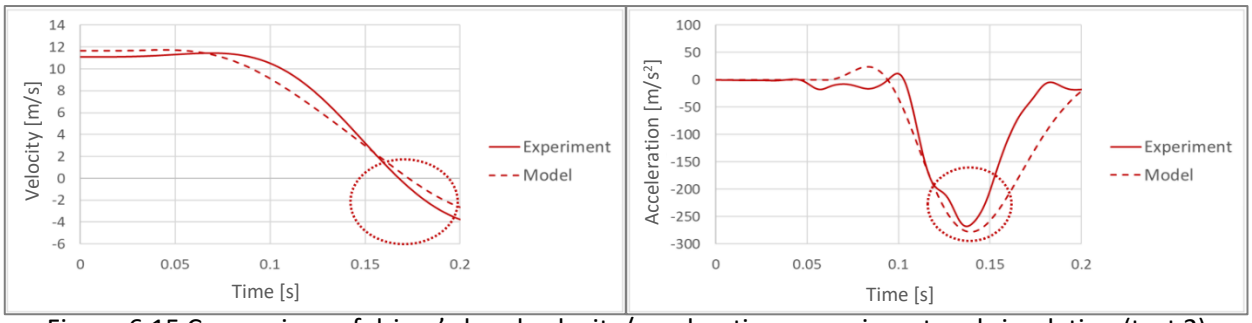

Figure 6.15 Comparison of driver's head velocity/acceleration: experiment and simulation (test 2)

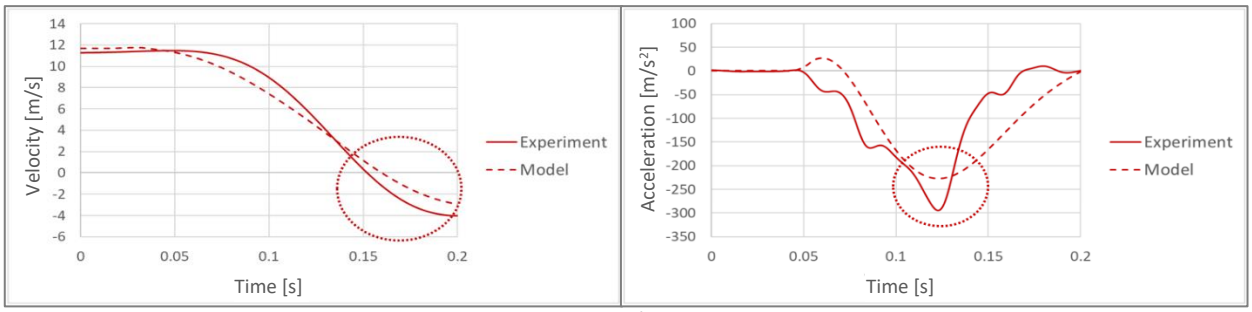

Figure 6.16 Comparison of driver's thorax velocity/acceleration: experiment and simulation (test 2)

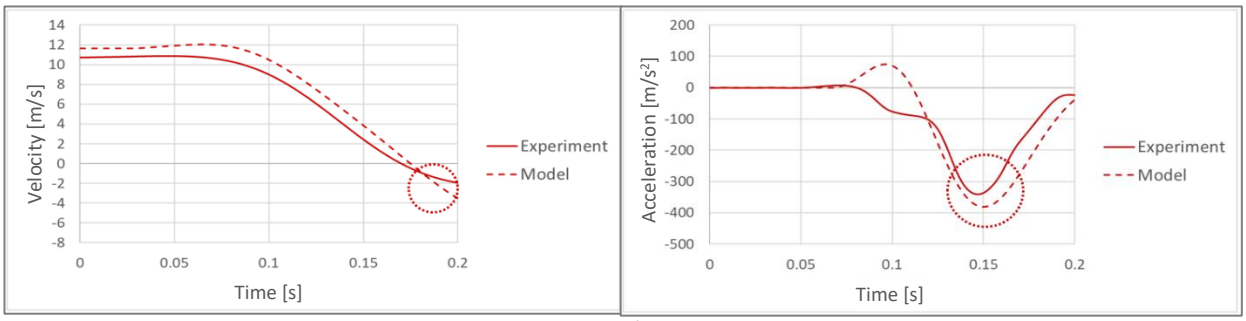

Figure 6.17 Comparison of passenger's head velocity/acceleration: experiment and simulation for test 2

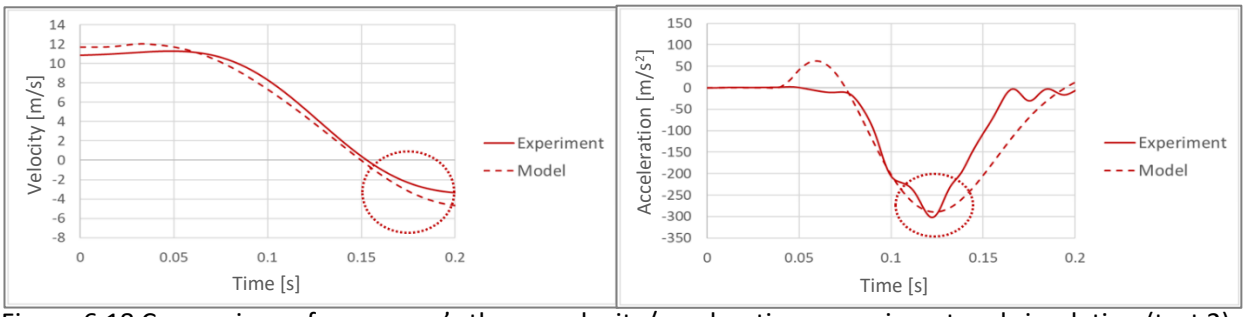

Figure 6.18 Comparison of passenger's thorax velocity/acceleration: experiment and simulation (test 2)

Even if the graphs differ greatly in their general appearance, the important aspect is that at extreme values, meaning the values of interest in experimental research, the curves are very close, or even overlap.

Calibration strengthened the validity of the model, providing it with extended applicability for predicting the dynamic behavior of the vehicle and its occupants under various experimental conditions. At the same time, simulations based on a single-occupant model proved suitable for experimental scenarios including two occupants (driver and passenger). The differences between the fractions determined in test 1 reflect the influence of the occupants' positions in the vehicle, while the uniformity in test 2 confirms the positive effect of damping on force distribution, both for the occupants and the vehicle structure.

6.4 Conclusions

The comparative analysis of the acceleration experienced by the occupants highlighted the efficiency of the energy-absorbing system in reducing impact forces on all axes (X, Y, and Z). In particular, the rear passenger was exposed to lower acceleration during the impact, which reflects the system's ability to mitigate the forces transmitted to him.

Although the energy-absorbing system led to an increase in vehicle acceleration on the Y and Z axes, the effect on both occupants was favorable. This suggests that, although the vehicle was subjected to higher vertical and lateral forces, the energy was distributed efficiently, protecting the occupants from head and thorax shocks.

However, the shock absorption system with water-filled plastic containers presents several limitations that affect its performance: water is incompressible, which reduces its shock-absorbing capacity, especially when the containers are completely filled; temperature variations influence the water's properties and may compromise system use (e.g. water can freeze, which limits use in low-temperature environments).

At the moment of collision, the water pressure inside the containers forming the energy-absorbing system exceeded the mechanical strength of the PET material (40–60 MPa), which caused them to burst [49]. Thus, the damping effect was generated by the yielding of the walls of the containers.

The analysis of the HIC 36 and ThAC injury criteria for dummies positioned in the driver's and rear passenger's seats highlighted the benefits of the energy-absorbing system, with improvements for the

passenger. Results indicate a reduction in HIC 36 values from 256.66 to 232.78 for the driver and from 493.39 to 229.14 for the rear passenger. ThAC values also decreased from 38.02 g (373 m/s²) to 30.92 g (303.3 m/s²) for the driver and from 45.14 g (442.8 m/s²) to 33.33 g (327 m/s²) for the passenger.

Regarding the probability of head injuries, it decreased from 1.60% to 1.47% for the driver and was significantly reduced for the passenger, from 3.60% to 1.45%. A similar trend is observed for thorax injuries, where the estimated probability decreased from 5.14% to 3.21% for the driver and from 8.15% to 3.77% for the passenger. These results confirm the effectiveness of the energy-absorbing system in improving the safety of the occupants.

In the absence of the shock absorption system, the average deformation of the affected area was 324.5125 mm, whereas in its presence, the value decreased to 237.4125 mm. By expanding the overall deformed area, the system reduces the direct load on the vehicle structure and contributes to efficient impact energy dissipation.

Validation of the mathematical model demonstrated consistency between simulated and experimental results for both the vehicle and its occupants (driver and passenger). The adjustments made by using fractions of the critical damping and by calibrating the time shifts allowed for an accurate representation of the system dynamics, highlighting both the influence of the occupants' positions and that of the energy-absorbing system on vehicle's behavior.

The analysis of percentage errors confirmed good correspondence between simulated and experimental results, demonstrating the model's accuracy in representing system dynamics. For test 1 (vehicle–rigid barrier), errors were 2.3% for the vehicle, 15.3% for the driver, and 9.5% for the passenger. In test 2 (vehicle with shock absorption system – rigid barrier), errors were 9.6% for the vehicle, 17.2% for the driver, and 10.1% for the passenger, maintaining the trend of lower values for the passenger.

The recalibrated intermediate fractions allowed for a balanced representation between the two tests, preserving the observed dynamic differences. The introduction of time shifts was essential for synchronizing the simulated responses with the experimental ones, consolidating the validity of the model.

In conclusion, the mathematical model proved to be a robust tool for analyzing the behavior of the vehicle and its occupants under various experimental conditions, providing a solid basis for future predictions and optimizations.

7 FINAL CONCLUSIONS. PERSONAL CONTRIBUTIONS. DISSEMINATION OF RESULTS. FUTURE RESEARCH DIRECTIONS

7.1 Final Conclusions

The research carried out within the doctoral thesis provides a complex perspective on road safety, with a focus on the frontal impact between a vehicle and a rigid barrier. Through an integrated approach combining theoretical analysis, mathematical modeling, numerical simulations, and experimental tests, interesting results were obtained for technical solutions that can be applied to improve occupant protection and optimize vehicle safety structures.

The analysis of the current state of research showed that road safety remains a global priority, and statistical analysis of accidents highlights both the progress made and the remaining challenges. Although a global decrease in road fatalities has been recorded, Romania continues to have a high rate of severe or fatal accidents, underlining the need for more effective prevention and intervention measures. Experimental research has advanced considerably, using sophisticated dummies such as THOR and Hybrid III, as well as sled testing technologies to better assess occupant protection. Integrating these tests with numerical simulations improved prediction accuracy, demonstrating the importance of a multidisciplinary approach to technical solutions aimed at reducing the risks associated with road accidents.

The theoretical study of collisions emphasized the importance of considering momentum conservation and the transformation of kinetic energy in structural deformation processes when analyzing technical solutions for mitigating occupant injuries during impact. Vehicle dynamics influence stability and control capability under critical conditions, while aerodynamic optimization contributes both to safety and energy efficiency. The vehicle's structural characteristics and the properties of materials used—such as HSLA and UHSLA steels, high-manganese steels, recyclable thermoplastics, and carbon fiber composites—influence the impact on the occupants. Biomechanical injury criteria allow for establishing limits for the forces exerted on the human body, forming the basis for the development of effective safety systems.

Based on the theoretical study, the research was directed toward achieving the established objectives, aiming to develop an energy-absorbing system to reduce the effects of collision on occupants. A mathematical model was developed to capture the behavior of the vehicle and its occupants during frontal impact, and its implementation enabled numerical simulation for evaluating kinematic parameters. Subsequently, the impact between the vehicle equipped with the energy-absorbing system and the rigid obstacle was simulated using the finite element method, determining the kinetic and internal energy values during the collision. The technical solution was materialized by designing and building the equipment intended to reduce collision effects. The experimental stage, carried out on physical models, provided the data necessary for evaluating injury criteria and validating the mathematical model.

The mathematical modeling study of the vehicle–rigid barrier impact demonstrated the relevance of correctly formulating the equations of motion to describe the dynamic phenomenon, using a system composed of masses, springs, and dampers. Implementing the model in Simulink made it possible to obtain time-dependent results for the kinematic parameters of both the vehicle and the occupants. A preliminary simulation, performed at an initial velocity of 60 km/h (16.7 m/s), verified the model responses before validation with experimental data. This revealed maximum decelerations of -283.7 m/s² (vehicle), -376.2 m/s² (thorax), and -448.6 m/s² (head). To extend this approach with advanced simulation methods, analytical methods such as Lagrange and Gibbs-Appell equations were used, allowing rigorous representation of multibody system dynamics. These techniques provide a mathematical framework for evaluating internal energy in safety structures. For this purpose, the vehicle was modeled with a shock absorption system consisting of 27 energy accumulators, without including the occupant. The 42 km/h impact simulation indicated an initial kinetic energy of 1.18×10^8 mJ. During the collision, this progressively decreased while the internal energy increased, becoming equal after 0.022 s. The internal energy continued to increase, reaching a maximum of 0.97×10^8 mJ at 0.06 s, at which point the kinetic

energy became negligible. In the analyzed nodes, displacements ranged from 105 mm to 227 mm, and velocities from 2.8 m/s to 11.1 m/s. Thus, by correlating analytical methods with advanced numerical simulation tools, the premises are created for a better understanding of the behavior of protection systems and for their optimization.

The acquisition and processing of experimental data represent an important stage in analyzing the vehicle–rigid barrier impact, contributing to the validation of theoretical models and optimization of collision scenarios. In this context, by using dedicated equipment and software applications, accurate data collection for vehicle and occupant kinematic parameters was ensured. Accelerations were measured using PicDAQ sensors, while velocity was determined through video analysis using the Tracker application. Implementing advanced filtering techniques increased the accuracy of results. By integrating equipment with software applications and data processing procedures, the rigor of the investigations was strengthened.

The experimental research methodology was designed to enable controlled and reproducible crash tests. The preparatory stages—including equipment calibration, verification of measurement systems, preparation of the vehicle and dummies, and determination of the parameters to be evaluated at the moment of impact—were important for result consistency. The implemented procedures allowed control of the impact variables and the acquisition of relevant experimental data necessary for a detailed analysis of vehicle and occupant behavior during collision.

The analysis performed after processing the experimental data confirmed the effectiveness of the shock absorption system in reducing the forces transmitted to the occupants, as evidenced by the reduction in head (HIC 36) and thorax (ThAC) injury criteria values. For the driver, the HIC 36 value was reduced from 256.66 to 232.78 (90.7% of the 256.66 value obtained in experimental testing without the shock absorption system), and the ThAC value from 38.02 g ≈ 373 m/s² to 30.92 g ≈ 303.3 m/s² (81.3%). For the rear passenger, a much more significant reduction was recorded, with HIC 36 decreasing from 493.39 to 229.14 (46.4%), and ThAC from 45.14 g ≈ 442.8 m/s² to 33.33 g ≈ 327 m/s² (73.8%). The probability of injury occurrence for the driver's head dropped from 1.60% to 1.47% and for the passenger's head from 3.60% to 1.45%, while for the thorax, from 5.14% to 3.21% in the first case and from 8.15% to 3.77% in the second. Validation of the mathematical model indicated good correlation between experimental and simulated results. For the vehicle–rigid barrier impact scenario, the errors were 2.3% (vehicle), 15.3% (driver), and 9.5% (passenger). For the test with the energy-absorbing system installed in the bumper, the recorded errors were: 9.6% for the vehicle, 17.2% for the driver, and 10.1% for the passenger. Using intermediate fractions and introducing time shifts allowed a more balanced adaptation of the model, with synchronized responses between experiments and simulations. Thus, it is found that the mathematical model is a useful tool in analyzing vehicle–rigid barrier impacts.

Based on the formulated conclusions, the thesis not only provides a technical solution applicable to reducing the severity of occupant injuries, but also proposes a rigorous methodology for impact analysis, thus contributing to the advancement of knowledge in the field of road safety.

7.2 Personal Contributions

This thesis brings original contributions in the field of vehicle safety research in the case of frontal collisions, combining mathematical modeling, experimental testing, and analysis of the obtained data to develop innovative occupant protection solutions. The main contributions are:

1. Development of a mathematical model for vehicle–rigid barrier impact

A three-degree-of-freedom mathematical model was developed. The model was created to provide a fast and accurate understanding of the interaction between the components involved in the impact.

2. Application of advanced analytical methods in mathematical modeling

Development of a numerical model for the frontal collision between a vehicle equipped with a damping system and a rigid barrier, using the finite element method. The model was discretized in Hypermesh. Running the analysis with the RADIOSS solver allowed a detailed evaluation of structural behavior in the post-processing stage, using the HyperView and HyperGraph software applications.

3. Designing and building an original energy-absorbing system for reducing occupant injuries

To mitigate the effects of the vehicle frontal collision and protect occupants, an innovative technical system was designed and built. The system was experimentally tested to evaluate its effectiveness in reducing accelerations and forces transmitted to the occupants.

4. Contributions to the determination of injury criteria for collision effect analysis

The thesis integrated the analysis of injury criteria to assess the severity of occupant injuries depending on the experimental configurations. This information is essential for improving vehicle safety measures.

5. Validation of the mathematical model

The mathematical model was validated by comparing the data resulting from simulations with those obtained from experimental tests.

6. Integration of numerical simulations and experimental data into a unified methodology

The research combined data obtained from numerical simulations and experimental tests to develop a robust methodology for analyzing vehicle–rigid barrier impacts. This methodology provides a framework for evaluating the effectiveness of impact attenuation systems and can be extended to other types of collisions.

7.3 Dissemination of Results

The dissemination of the results obtained from the research was an important aspect in the phase of presenting the author's own scientific contributions. In this respect, academic and professional communication channels were used, including the publication of articles and participation in international conferences.

Over the five years of study at the Doctoral School of Transilvania University of Brașov and of scientific activity, the author published eight papers as first author and five as co-author, in which original results were presented. Six articles were published in ISI-ranked journals. Another four articles were presented at international conferences and indexed by ISI. They contributed to promoting the research and presenting the methodologies and conclusions obtained from the studies. Two papers were included in international bibliographic databases (BDI). One article was included in the proceedings of an international conference, ensuring wide dissemination of the results in the academic community.

7.4 Future Research Directions

The results and conclusions obtained in the thesis open opportunities for extending research in several directions relevant to the field of road safety. Among these are:

1. Extending the applicability of the mathematical model to other types of collisions

Development and validation of similar mathematical models for other types of impacts, such as side or rear collisions, to analyze vehicle structural behavior and occupant kinematics.

2. Analysis of the influence of deformations on occupant protection

Research on how the car body absorbs and distributes impact energy to protect occupants.

3. Development of new experimental research methods

Use of equipment and methods that allow measurement of forces applied to the occupant's neck and thorax, as well as recording their deformations during an impact. In addition, by using advanced technologies such as next-generation sensors and AI-based systems, the collection and processing of experimental data can be improved.

4. Investigation of alternative energy-absorbing solutions

Development of energy-absorbing systems based on innovative materials and technologies, combining performance with reduced weight and increased reliability. Future research could explore the use of magnetorheological fluids or materials with enhanced energy absorption properties, offering safer and more efficient solutions for vehicle occupant protection.

5. Optimization of the technical energy-absorbing solution for different impact scenarios

Adjusting and testing the shock absorption system to ensure optimal performance depending on collision velocity and type, as well as meeting specific requirements.

6. Research on the influence of partial liquid filling of containers to create an advanced shock absorption system

Since fully filled containers limit energy-absorbing capacity, future research should focus on solutions based on progressive partial filling (e.g., 70%, 80%, 90%). The properties of water vary significantly with temperature, which affects the overall behavior of the shock absorption system and requires careful consideration when selecting the liquid used. Both the use of water and the testing of liquids with variable viscosity and antifreeze properties will be pursued to ensure efficient system operation under various conditions.

7. Analysis of how the size and configuration of the orifices of the containers influence shock absorption at the moment of impact and occupant protection

Research focuses on how the size and configuration of the orifices of the containers control the liquid flow and contribute to dissipating the impact energy, ensuring occupant protection.

SELECTIVE BIBLIOGRAPHY

[1] American National Standards Institute. (2017). Manual on classification of motor vehicle traffic crashes. ANSI D16-2017, pp. 19–20.

[2] Comisia Europeană (2024). ERSO Country Overview 2024: Romania. European Road Safety Observatory. Disponibil la: https://road-safety.transport.ec.europa.eu.

[3] Organizația Mondială a Sănătății. (2023). Global status report on road safety 2023. Geneva: World Health Organization. Disponibil la: https://www.who.int/publications/i/item/9789240086517.

[4] Insurance Institute for Highway Safety. (2022). Collisions with fixed objects and animals. Disponibil la: https://www.iihs.org/topics/fatality-statistics/detail/collisions-with-fixed-objects-and-animals.

[5] Björnberg, E., Hansson, S. O., Belin, M. Å., & Tingvall, C. (2023). The Vision Zero Handbook. Cham, Switzerland: Springer International Publishing, p. 755.

[6] Das, S., Geedipally, S. R., Dixon, K., Sun, X., & Ma, C. (2019). Measuring the effectiveness of vehicle inspection regulations in different states of the US. Transportation research record, 2673(5), pp. 208-219.

[7] Freund, D. M. (2007). Foundations of Commercial Vehicle Safety: Laws, Regulations, and Standards. SAE International, pp. 1-22.

[8] Blomquist, G. C. (2012). The regulation of motor vehicle and traffic safety. Springer Science & Business Media, p. 11.

[9] Gonter, M., & Seiffert, U. W. (2013). Integrated automotive safety handbook. SAE international, pp. 6-11.

[10] Alhaddad, A. Y., Cabibihan, J. J., Hayek, A., & Bonarini, A. (2019). A low-cost test rig for impact experiments on a dummy head. HardwareX, 6, e00068.

[11] Gu, H., Lou, L., & Jiang, X. (2020). Injury Characteristics of Different Dummies Based on Frontal Impact Test. In Big Data Analytics for Cyber-Physical System in Smart City: BDCPS 2019, 28-29 December 2019, Shenyang, China. Springer Singapore, pp. 1347-1354.

[12] Untaroiu, C. D., Shin, J., & Lu, Y. C. (2013). Assessment of a dummy model in crash simulations using rating methods. International Journal of Automotive Technology, 14, pp. 395-405.

[13] Fung, K., Xu, R., Jung, S., & Sobanjo, J. (2019). Development and testing of a simplified dummy for frontal crash. Experimental Techniques, 43, pp. 7-14.

[14] Summers, S., Hall, I., Parent, D., & Keon, T. (2021). Occupant Response Evaluation in Flat, Full-Frontal Rigid Barrier Impact Testing (No. DOT HS 813 014). United States. Department of Transportation. National Highway Traffic Safety Administration.

[15] Untaru, M., Stoicescu, A., Poțincu, Gh., Pereș, Gh., & Tabacu, I. (1981). Dinamica autovehiculelor pe roți. Editura Didactică și Pedagogică, pp. 156-160.

[16] Ogura, A. (2017). Analyzing collisions in classical mechanics using mass–momentum diagrams. European Journal of Physics, 38(5), 055001, p. 2.

[17] Stronge, W. J. (2018). Impact mechanics. Cambridge university press, pp. 23-24.

[18] Tang, X. H., Paluszny, A., & Zimmerman, R. W. (2013). Energy conservative property of impulse-based methods for collision resolution. International journal for numerical methods in engineering, 95(6), pp. 529-540.

[19] Reed, B. C. (2018). A compact general expression for momentum exchange in elastic collisions. American Journal of Physics, 86(8), pp. 622-622.

[20] Rosenthal, F., Bort, R. L., O'Hara, G. J., Clements, E. W., & Skop, R. A. (1972). The Mechanics of Automobile Collisions. NRL Memoran-dum Report, p. 51.

[21] Heißing, B., & Ersoy, M. (Eds.). (2010). Chassis handbook: fundamentals, driving dynamics, components, mechatronics, perspectives. Springer Science & Business Media, p. 1.

[22] Șoica, A. (2017). Caroserii și sisteme de siguranță pasivă [Suport de curs]. Brașov.

[23] Grzebieta, R. H., Zou, R., Jiang, T., & Carey, A. (2005). Roadside hazard and barrier crashworthiness issues confronting vehicle and barrier manufactures and government regulators. In Proc. 19th International technical conference on the enhanced safety of vehicles, Washington, USA.

[24] Liščák, Š., & Moravčík, Ľ. (2013). Safety requirements for road vehicles. Perner's Contacts, 8(4), pp. 49-59.

[25] Backaitis, S. H., DeLarm, L., & Robbins, D. H. (1982). Occupant kinematics in motor vehicle crashes (No. 820247). SAE Technical Paper.

[26] Karapetkov, S., Uzunov, H., Dechkova, S., & Uzunov, V. (2023). Impact of inertial forces on car occupants in a vehicle-fixed barrier front crash. Symmetry, 15(11), 1998.

[27] Schmitt, K. U., Niederer, P. F., Cronin, D. S., Morrison III, B., Muser, M. H., & Walz, F. (2019). Trauma biomechanics: an introduction to injury biomechanics. Springer, p. 24.

[28] Chell, J., Brandani, C. E., Fraschetti, S., Chakraverty, J., & Camomilla, V. (2019). Limitations of the European barrier crash testing regulation relating to occupant safety. Accident Analysis & Prevention, 133, 105239.

[29] Roque, C., & Cardoso, J. L. (2013). Observations on the relationship between European standards for safety barrier impact severity and the degree of injury sustained. IATSS research, 37(1), pp. 21-29.

[30] Deac, S. C., Perescu, A., Simoiu, D., Nyaguly, E., Crâştiu, I., & Bereteu, L. (2018). Modeling and simulation of cars in frontal collision. In IOP Conference Series: Materials Science and Engineering. IOP Publishing, Vol. 294, No. 1.

[31] Eshkabilov, S. (2019). Beginning MATLAB and simulink: From novice to professional. Apress, pp. 1-2, 275-280.

[32] Eshkabilov, S. L. (2020). Practical MATLAB Modeling with Simulink. Apress, Springer.

[33] Nedelescu, C., Vrabie, P., Garnita, I. A., Trusca, D., & Chiru, A. (2020). Investigation of deformations in the scenario of an impact with a rigid barrier. În COMAT 2020, ISSN 2457-8541. Editura Universității Transilvania din Brașov.

[34] Mizuno, K., Nezaki, S., & Ito, D. (2017). Comparison of chest injury measures of hybrid III dummy. International Journal of Crashworthiness, 22(1), pp. 38-48.

[35] Schmidt, A. L., Ortiz-Paparoni, M. A., Shridharani, J. K., Nightingale, R. W., & Bass, C. R. (2018). Time and temperature sensitivity of the Hybrid III neck. Traffic injury prevention, 19(6), pp. 657-663.

[36] Vlase, S., Negrean, I., Marin, M., & Scutaru, M. L. (2020). Energy of accelerations used to obtain the motion equations of a three-dimensional finite element. Symmetry, 12(2), 321.

[37] Ursu-Fisher, N. (2015). Elements of analytical mechanics. House of Science Book Press.

[38] Krauklis, A. E., Gagani, A. I., & Echtermeyer, A. T. (2019). Prediction of orthotropic hygroscopic swelling of fiber-reinforced composites from isotropic swelling of matrix polymer. Journal of Composites Science, 3(1), 10.

[39] Covaciu, D., Preda, I., Ciolan, G., & Câmpian, O. V. (2010). Data acquisition system based on GPS technology, for vehicle dynamics analysis. În CONAT 2010, Universitatea Transilvania din Brașov.

[40] DSD. (n.d.). PicDAQ – Fișa tehnică. Accesată pe 3 iunie 2024, la: http://www.dsd.at/index.php?option=com_content&view=article&id=16:pic-daq&catid=37&Itemid=159&lang=en.

[41] Dima, D. S., & Covaciu, D. (2017). Solutions for acceleration measurement in vehicle crash tests. In IOP Conference Series: Materials Science and Engineering (Vol. 252, No. 1). IOP Publishing.

[42] Physlets. (n.d.). Tracker Video Analysis and Modeling Tool – Pagina principală. Accesată pe 25 iulie 2024, la: https://physlets.org/tracker/.

[43] Ahmed, A., Sadullah, A. F. M., & Yahya, A. S. (2019). Errors in accident data, its types, causes and methods of rectification-analysis of the literature. Accident Analysis & Prevention, 130, pp. 3-21.

[44] Wang, X., Liu, Q., Guo, F., Xu, X., & Chen, X. (2022). Causation analysis of crashes and near crashes using naturalistic driving data. Accident Analysis & Prevention, 177, 106821. Elsevier.

[45] Brach, M., Mason, J., & Brach, R. M. (2022). Vehicle accident analysis and reconstruction methods. SAE international, pp. 1-3.

[46] OriginLab. (n.d.). Pagina principală. Accesată pe 3 iunie 2024, la: https://www.originlab.com/.

[47] Fastec Imaging. (n.d.). HiSpec 5 – Fișa tehnică. Accesată pe 20 ianuarie 2025, la: http://upd.fastecimaging.com/docs/Datasheets/hispec5.pdf.

[48] DJI. (n.d.). Phantom 3 Standard – Fișă tehnică. Accesată pe 21 ianuarie 2025, la: https://www.dji.com/global/support/product/phantom-3-standard.

[49] Salama, E. S., & Summers, J. K. (2023). Advances and Challenges in Microplastics. IntechOpen.